NASA TECHNICAL NOTE

NASA TN D-6439

SIMILAR SOLUTIONS FOR TURBULENT BOUNDARY LAYER WITH LARGE FAVORABLE PRESSURE GRADIENTS (NOZZLE FLOW WITH HEAT TRANSFER)

by James F. Schmidt, Donald R. Boldman, and Carroll Todd

Lewis Research Center
Cleveland, Ohio 44135

NATIONAL AERONAUTICS AND SPACE ADMINISTRATION • WASHINGTON, D. C. • AUGUST 1971

1. Report No. NASA TN D-6439	2. Government Accession No.	3. Recipient's C...
4. Title and Subtitle SIMILAR SOLUTIONS FOR TURBULENT BOUNDARY LAYER WITH LARGE FAVORABLE PRESSURE GRADIENTS (NOZZLE FLOW WITH HEAT TRANSFER)		5. Report Date August 1971 6. Performing Organization Code
7. Author(s) James F. Schmidt, Donald R. Boldman, and Carroll Todd		8. Performing Organization Report No. E-6109
9. Performing Organization Name and Address Lewis Research Center National Aeronautics and Space Administration Cleveland, Ohio 44135		10. Work Unit No. 120-27 11. Contract or Grant No.
12. Sponsoring Agency Name and Address National Aeronautics and Space Administration Washington, D.C. 20546		13. Type of Report and Period Covered Technical Note 14. Sponsoring Agency Code
15. Supplementary Notes		

16. Abstract

In order to provide a relatively simple heat-transfer prediction along a nozzle, a differential (similar-solution) analysis for the turbulent boundary layer is developed. This analysis along with a new correlation for the turbulent Prandtl number gives good agreement of the predicted with the measured heat transfer in the throat and supersonic region of the nozzle. Also, the boundary-layer variables (heat transfer, etc.) can be calculated at any arbitrary location in the throat or supersonic region of the nozzle in less than a half minute of computing time (Lewis DCS 7094-7044).

17. Key Words (Suggested by Author(s)) Fluid mechanics Boundary layer Heat transfer	18. Distribution Statement Unclassified - unlimited		
19. Security Classif. (of this report) Unclassified	20. Security Classif. (of this page) Unclassified	21. No. of Pages 63	22. Price* $3.00

*For sale by the National Technical Information Service, Springfield, Virginia 22151

SIMILAR SOLUTIONS FOR TURBULENT BOUNDARY LAYER WITH LARGE FAVORABLE PRESSURE GRADIENTS (NOZZLE FLOW WITH HEAT TRANSFER)

by James F. Schmidt, Donald R. Boldman, and Carroll Todd

Lewis Research Center

SUMMARY

In order to provide a relatively simple heat-transfer prediction along a nozzle, a differential (similar-solution) analysis for the turbulent boundary layer is developed. This analysis along with a new correlation for the turbulent Prandtl number gives good agreement of the predicted with measured heat transfer in the throat and supersonic region of the nozzle. Also, the boundary-layer variables (heat transfer, etc.) can be calculated at any arbitrary location in the throat or supersonic region of the nozzle in less than a half minute of computing time (Lewis DCS 7094-7044). For example, the boundary layer at the nozzle exit location can be calculated directly without the requirement of the usual step-by-step marching calculation method for the complete nozzle boundary layer.

This analysis is applied to a cooled 30° convergent, 15° divergent conical nozzle with cooled and uncooled inlets for comparison with experimental measurements. Except for the low subsonic-flow region of the nozzle, the theoretical predictions are in good agreement with experimental data.

INTRODUCTION

The present (similar-solution) analysis is an approximate calculation of the turbulent differential boundary-layer equations for nozzle flow. This report presents a relatively simple calculation method as compared with differential finite-difference calculation methods for predicting a reliable heat transfer distribution along the nozzle.

Both finite-difference and integral calculation methods require a step-by-step marching calculation technique starting from the nozzle entrance to the desired nozzle location. Therefore, if one is only interested in, for example, the nozzle exit location,

these step by step marching methods require that the complete nozzle boundary-layer be calculated. However, this similar-solution analysis has the advantage of being able to directly calculate this nozzle location or any arbitrary location in the throat or supersonic region using only a half minute of computing time.

In the past, the turbulent integral boundary-layer theory of Bartz (ref. 1) is the method most often used for predicting the heat transfer in nozzle flows. This integral analysis provides reasonably fair predictions of throat heat transfer when the momentum thickness Reynolds number is replaced by the energy thickness Reynolds number in the momentum-heat analogy.

In more recent years, several differential numerical calculation methods have been developed for the turbulent boundary layer (refs. 2 to 5). All these calculation methods use an eddy diffusivity concept and a finite-difference calculation procedure. However, only Bushnell and Beckwith (ref. 5) have applied a finite-difference analysis to a nozzle flow calculation (according to the current published literature). Their calculation was initiated at the nozzle throat and proceeded downstream with the primary purpose of calculating the boundary-layer velocity and temperature profile at the nozzle exit for comparison with measured profiles. One interesting point to note from their nozzle calculation is that a constant turbulent Prandtl number of 1.5 or more was necessary for good agreement of the theoretical with the measured nozzle-exit boundary-layer profiles. This large value of the turbulent Prandtl number is unusual because it indicates a much lower turbulent heat transport than momentum transport. However, it is important to realize that this turbulent Prandtl number from reference 5 is based on the total enthalpy gradient and not the usual static enthalpy (temperature) gradient. Actually, in supersonic flow one might expect a significantly different value of Pr_T (based on total enthalpy) than the usually assumed value of 0.90 (Pr_T) based on static enthalpy), because the kinetic energy now becomes a large percentage of the total enthalpy. Irrespective of whether the turbulent Prandtl number is based on the static or total enthalpy gradient, there are presently no direct measurements available to determine the turbulent Prandtl number in compressible boundary-layer flows.

This discussion of the turbulent Prandtl number is intended to emphasize the fact that not even a rough approximation for Pr_T is available for nozzle flows. In addition, the predicted nozzle heat transfer is expected to be strongly dependent on the assumed Pr_T. In the present analysis the turbulent Prandtl number (based on the total enthalpy gradient) is correlated to approximate the strong streamwise variation of Pr_T along the nozzle that is necessary for favorable agreement of the predicted with experimental heat transfer data (refs. 6 to 8).

Unlike the finite-difference calculation methods (refs. 2 to 5), the present analysis is an underrelaxed successive approximation, similar-solution calculation of the turbulent differential, boundary-layer equations. A Howarth-Doronitsyn compressibility

type of transformation along with a new transformation on the dependent similarity variables reduce the form of the nonlinear, differential, boundary-layer equations to ordinary differential equations. A three layer model is assumed for the eddy diffusivity which consists of a laminar sublayer region developed by Deissler (ref. 9), a law of the wall region described by Prandtl's mixing length theory (ref. 10) and an outer intermittency region given by Clauser's approximation (ref. 11).

The results of this analysis are compared with the experimental boundary-layer and heat-transfer measurements of references 6 to 8, which were obtained for cooled conical nozzles with cooled and uncooled inlets. The experimental data used for this comparison are taken from tests conducted with heated air at a nominal stagnation temperature of 539 K (970° R) and nominal stagnation pressures of 207 newtons per square centimeter (300 psia) and 20.65 newtons per square centimeter (30 psia) for the nozzle with a convergent half angle of 30° and divergent half angle of 15°. The present analysis is also compared with the turbulent integral boundary-layer theory of Bartz (ref. 1).

ANALYSIS

Assumptions

(1) Axisymmetric, steady, nozzle flow is assumed.

(2) Surface curvature is neglected in the boundary-layer equations.

(3) Pressure is constant across the boundary layer.

(4) The eddy diffusivity concept is applicable for nozzle flows.

(5) The eddy diffusivity relations developed for zero pressure gradient, incompressible, turbulent boundary layers are assumed to be applicable for highly accelerated compressible turbulent boundary layers.

(6) Local similarity is assumed in the solution of the turbulent boundary-layer equations.

(7) The turbulent Prandtl number (based on the total enthalpy gradient) is constant across the boundary layer but has a large variation along the nozzle.

Basic Equations

From appendix B, the following system of turbulent, compressible, boundary-layer equations for axisymmetric steady-flow can be expressed (in terms of the eddy diffusivity concept) as

Continuity

$$(\rho ur)_x + (\rho vr)_y = 0 \tag{1}$$

Momentum

$$\rho u\, u_x + \rho v u_y = \rho_e u_e (u_e)_x + \left[(\mu + \rho\epsilon_m)u_y\right]_y \tag{2}$$

Energy

$$\rho u H_x + \rho v H_y = \left[\left(\frac{\mu}{Pr_L} + \rho\frac{\epsilon_m}{Pr_T}\right)H_y\right]_y + \left[\mu\left(1 - \frac{1}{Pr_L}\right)\left(\frac{u^2}{2}\right)_y\right]_y \tag{3}$$

State

$$P = \rho \mathscr{R} T \tag{4}$$

(All symbols are defined in appendix A.)

The boundary-layer coordinate system along the cylindrical pipe inlet and 30° nozzle is shown in figure 1.

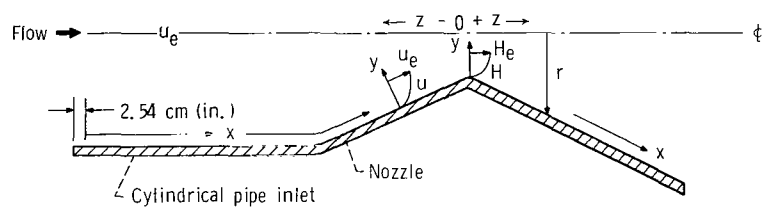

Figure 1. - Boundary layer coordinate system along pipe inlet and 30° nozzle.

The dimensions for the conical nozzle with a convergent half angle of 30° and a divergent half angle of 15° are given in table I.

Before these boundary layer equations (eqs. (1) to (3)) can be solved, expressions for the momentum eddy diffusivity and for the turbulent Prandtl number Pr_T are needed. As discussed in the INTRODUCTION, a three-layer model is assumed for the momentum eddy diffusivity. The momentum eddy diffusivity for the laminar sublayer region is given by Deissler (ref. 9) as

$$\epsilon_{m,1} = n^2 uy \tag{5}$$

The momentum eddy diffusivity for the "law of the wall" region is given by the following Prandtl expression (ref. 10):

$$\epsilon_{m,2} = \kappa^2 y^2 u_y \tag{6}$$

Clauser's approximation (ref. 11) for the eddy diffusivity in the outer intermittency region is given by

$$\epsilon_{m,3} = \zeta u_e \delta_i^* \tag{7}$$

where n, κ, and ζ are experimental flow constants based on low speed incompressible displacement thickness, δ_i^*, is

$$\delta_i^* = \int_0^{y_\infty} \left(1 - \frac{u}{u_e}\right) dy \tag{8}$$

The turbulent Prandtl number Pr_T is assumed to be constant across the boundary layer. The molecular or laminar Prandtl number Pr_L is assumed to be constant at 0.71, and the viscosity is approximated by

$$\mu = \mu_0 \left(\frac{t}{T_0}\right)^d = \mu_0 \left(\frac{h}{H_0}\right)^d \tag{9}$$

where the specific heat at constant pressure c_p is assumed constant because of the low temperatures considered in this analysis (perfect gas).

Transformed Equations

Using a Howarth-Doronitsyn compressibility type of transformation, which is essentially identical to Smith's transformation (ref. 2), the following transformation equations used in solving the boundary-layer equations (1) to (3) are

$$\eta = \frac{\rho_e (u_e)^{1/2}}{(\rho_0 \mu_0 2\tilde{x})^{1/2}} \int_0^y \frac{\rho}{\rho_e} dy \tag{10a}$$

where

$$\tilde{x} = x \tag{10b}$$

The partial derivatives transform as follows:

$$( )_y = \frac{\rho u_e^{1/2}}{(\rho_0 \mu_0 2\tilde{x})^{1/2}} ( )_\eta \tag{10c}$$

$$( )_x = ( )_{\tilde{x}} + ( )_\eta \eta_{\tilde{x}} \tag{10d}$$

From continuity the stream function ψ is defined such that

$$\rho u r = (\psi r)_y \tag{10e}$$

$$\rho v r = -(\psi r)_x \tag{10f}$$

By letting

$$\psi = (\rho_0 \mu_0 2\tilde{x} u_e)^{1/2} f(\eta, \tilde{x}) \tag{10g}$$

then

$$f_\eta = \frac{u}{u_e} \tag{10h}$$

Also let

$$g = \frac{H}{H_0} \tag{10i}$$

Applying the transformation equations (10) to the momentum and energy equations (2) and (3), assuming local similarity, and reducing gives

Momentum

$$\left\{\left[C + D_1\left(\frac{\rho}{\rho_e}\right)^2 \epsilon_m\right] f_{\eta\eta}\right\}_\eta + D_2 f f_{\eta\eta} = -\beta\left[\frac{1}{\rho/\rho_e} - (f_\eta)^2\right] \tag{11}$$

Energy

$$\left\{\left[\frac{C}{Pr_L} + D_1\left(\frac{\rho}{\rho_e}\right)^2 \frac{\epsilon_m}{Pr_T}\right] g_\eta\right\}_\eta + D_2 f g_\eta = -2D_3\left[C\left(1 - \frac{1}{Pr_L}\right) f_\eta f_{\eta\eta}\right]_\eta \tag{12}$$

The parameters in equations (10) and (11) are now derived. The density-viscosity ratio C is defined as

$$C = \frac{\rho\mu}{\rho_0\mu_0} = \frac{P_e}{P_0}\frac{T_0}{T}\frac{\mu}{\mu_0} \tag{13}$$

Using equations (9) and (10f) with the definition of total enthalpy in equation (13) and and reducing result in the transformed density-viscosity ratio

$$C = \frac{P_e}{P_0}\left\{\frac{1}{\left[g - D_3(f_\eta)^2\right]}\right\}^{1-d} \tag{14}$$

and for D_3, the ratio of kinetic to total energy,

$$D_3 = \frac{u_e^2}{2H_0} \tag{15}$$

The density ratio ρ/ρ_e can be expressed as

$$\frac{\rho}{\rho_e} = \frac{t_e}{t} = \frac{h_e}{h} = \frac{1 - D_3}{g - D_3(f_\eta)^2} \tag{16}$$

The flow coefficients D_1 and D_2 are

$$D_1 = \frac{\rho_e^2}{\rho_0 \mu_0} \tag{17}$$

$$D_2 = 1 + \frac{\beta}{2} + R \tag{18}$$

where β, the velocity gradient parameter, is

$$\beta = \frac{2\tilde{x}}{u_e}\left(u_e\right)_{\tilde{x}} \tag{19}$$

and $\tilde{x}$ is the turbulent boundary layer, distance coordinate starting at the origin of the turbulent boundary layer (approximately 2.54 cm (1 in.) inside the cylindrical inlet).

The nozzle geometry parameter R is defined as

$$R = \frac{2\tilde{x}}{r}\left(r\right)_{\tilde{x}} \tag{20}$$

Some of these boundary-layer parameters such as β, R, D_3, etc., are tabulated for each measuring station along the nozzle in table II.

With the substitution of the transformation equations (10) in equations (5) to (7) and reducing, the transformed momentum eddy diffusivity for each region becomes

Laminar sublayer region

$$\epsilon_{m,1} = n^2 \frac{(\rho_0 \mu_0 2\tilde{x} u_e)^{1/2}}{\rho_e} f_\eta \int_0^\eta \frac{d_\eta}{\rho/\rho_e} \tag{21}$$

Law of the wall region

$$\epsilon_{m,2} = \kappa^2 \left(\frac{\rho}{\rho_e}\right) \frac{(\rho_0 \mu_0 2\tilde{x} u_e)^{1/2}}{\rho_e} f_{\eta\eta} \left[\int_0^\eta \frac{d_\eta}{(\rho/\rho_e)}\right]^2 \tag{22}$$

Outer intermittency region

$$\epsilon_{m,3} = \zeta \frac{(\rho_0 \mu_0 2 \tilde{x} u_e)^{1/2}}{\rho_e} \int_0^{\eta} \frac{(1 - f_\eta)}{\rho/\rho_e} d\eta \tag{23}$$

The assumed criteria for switching from the laminar sublayer region to the law of the wall region is at $y^+ = 12$. The criteria for switching from the law of the wall to the outer intermittency region is when the ratio of the eddy-diffusivity for the law of the wall to the intermittency region is one. This wall distance parameter y^+ is defined (ref. 9) as

$$y^+ = \frac{y\left(\frac{\tau_w}{\rho_w}\right)^{1/2}}{\frac{\mu_w}{\rho_w}} = \frac{y\, u_e}{\frac{\mu_w}{\rho_w}} \left(\frac{C_f}{2} \frac{\rho_e}{\rho_w}\right)^{1/2} \tag{24}$$

The turbulent Prandtl number Pr_T is, by definition,

$$Pr_T = \frac{\epsilon_m}{\epsilon_H} \tag{25}$$

As mentioned in the INTRODUCTION, the turbulent Prandtl number is assumed constant across the boundary layer but is correlated (purely by numerical experience) to provide the proper x-streamwise variation of Pr_T for good agreement of the theoretical with measured nozzle heat transfer.

The correlation for Pr_T is

$$Pr_T = (D_2)^{1/2} = \left(1 + \frac{\beta}{2} + R\right)^{1/2} \tag{26}$$

In order to simplify the numerical calculations and provide a finite boundary condition at the edge of the boundary layer, the following independent variable transformation is applied to the momentum and energy equations:

$$\gamma = \frac{\eta}{\delta} \tag{27}$$

where δ is equal to η_∞ (the boundary-layer thickness in the η-coordinate).

Substituting equation (27) in equations (11) and (12), the momentum and energy equations in the γ-system become

Momentum

$$\left\{\left[C + D_1\left(\frac{\rho}{\rho_e}\right)^2 \epsilon_m\right] f_{\gamma\gamma}\right\}_\gamma + \delta D_2 f f_{\gamma\gamma} = -\delta^3 \beta\left[\frac{1}{\rho/\rho_e} - \left(\frac{f_\gamma}{\delta}\right)^2\right] \tag{28}$$

Energy

$$\left\{\left[\frac{C}{Pr_L} + D_1\left(\frac{\rho}{\rho_e}\right)^2 \frac{\epsilon_m}{Pr_T}\right] g_\gamma\right\}_\gamma + D_2 \delta f g_\gamma = -\frac{2D_3}{\delta^2}\left\{C\left(1 - \frac{1}{Pr_L}\right) f_\gamma f_{\gamma\gamma}\right\}_\gamma \tag{29}$$

Using the following dependent variable transformation, similar to appendix B of reference 12, eliminates the need for numerically differentiating the eddy diffusivity as well as the flow properties across the boundary layer:

$$\mathscr{P}_f = \overline{C}_1 f_{\gamma\gamma} \tag{30}$$

$$\mathscr{P}_g = \overline{C}_2 g_\gamma \tag{31}$$

The transformation coefficients $\overline{C}_1$ and $\overline{C}_2$ are

$$\overline{C}_1 = C + D_1\left(\frac{\rho}{\rho_e}\right)^2 \epsilon_m \tag{32}$$

$$\overline{C}_2 = \frac{C}{Pr_L} + D_1\left(\frac{\rho}{\rho_e}\right)^2 \frac{\epsilon_m}{Pr_T} \tag{33}$$

Substituting equations (30) to (33) into equations (28) to (29) and reducing, the momentum and energy equations become

Momentum

$$\left(\mathscr{P}_f\right)_\gamma + \delta D_2 \frac{f}{\overline{C}_1}\mathscr{P}_f = -\delta^3\beta\left[\frac{1}{\rho/\rho_e} - \left(\frac{f_\gamma}{\delta}\right)^2\right] \tag{34}$$

Energy

$$\left(\mathscr{P}_g\right)_\gamma + \delta D_2 \frac{f}{\overline{C}_2}\mathscr{P}_g = -\frac{2D_3}{\delta^2}\left[C\left(1 - \frac{1}{Pr_L}\right)f_\gamma f_{\gamma\gamma}\right]_\gamma \tag{35}$$

The momentum and energy equations (34) and (35) now have the form of ordinary differential equations of the first order:

Momentum

$$\left(\mathscr{P}_f\right)_\gamma + A_M\mathscr{P}_f = B_M \tag{36}$$

Energy

$$\left(\mathscr{P}_g\right)_\gamma + A_E\mathscr{P}_g = B_E \tag{37}$$

where

$$A_M = D_2\delta\frac{f}{\overline{C}_1} \tag{38}$$

$$B_M = -\delta^3\beta\left[\frac{1}{\rho/\rho_e} - \left(\frac{f_\gamma}{\delta}\right)^2\right] \tag{39}$$

$$A_E = D_2\frac{\delta f}{\overline{C}_2} \tag{40}$$

$$B_E = -\frac{2D_3}{\delta^2}\left\{C\left(1 - \frac{1}{Pr_L}\right)f_\gamma f_{\gamma\gamma}\right\}_\gamma \tag{41}$$

The following boundary conditions are applied to equations (38) and (39):

$$\left.\begin{aligned} &\text{at } \gamma = 0 \\ &\qquad f = f_\gamma = 0 \text{ and } (g)_{\gamma=0} = g_w \\ &\text{at } \gamma = 1.0 \\ &\qquad f_\gamma = \delta, \qquad g = 1.0 \\ &\qquad \frac{f_{\gamma\gamma}}{\delta^2} < 10^{-3} \text{ and } \frac{g_\gamma}{\delta} < 10^{-3} \end{aligned}\right\} \tag{42}$$

Solutions of the momentum and energy equations (36) and (37) with their respective boundary conditions (42) are obtained for the conical nozzle using measured wall temperatures and pressure distribution along the nozzle (ref. 6). All the boundary-layer functions and flow coefficients are transferred back into the η-system after the solutions are obtained.

Numerical Complications

Boundary-layer equations (1) to (3) for a compressible gas in accelerated nozzle flow form a set of highly nonlinear partial differential equations. Not only does this nonlinearity (which increases with increase in the pressure gradient) cause numerical instabilities in most numerical procedures, but also the momentum and energy equations are coupled. The nonlinearity and strong coupling of the energy to the momentum equation primarily results from variable gas properties and high flow velocities. To further complicate the numerical calculation, the boundary-layer problem is a two-point boundary problem but one boundary condition is at infinity ($\eta = \infty$).

In order to circumvent some of these difficulties, a new independent variable (γ-system) and two new dependent variables (eqs. (30) and (31)) are used to reduce the form of the equations to a set of ordinary differential equations that can more easily be solved. Now the numerical system has a finite boundary condition at the edge of the boundary layer ($\gamma = 1.0$). This numerical system is an underrelaxed, successive-approximation calculation with a unique "stepping-up process," which is essentially a sequence of boundary-layer solutions from a greatly reduced boundary-layer thickness to the actual edge of the boundary layer. First a boundary-layer thickness δ (in the η-coordinate), which is much smaller than the expected boundary-layer thickness is chosen. Then the

boundary-layer equations are solved (see appendix C and fig. 19) and the derivatives ($f_{\gamma\gamma}/\delta^2$ and g_γ/δ) at the edge of the assumed layer are checked to see if the values of these derivatives are within the specified limits ($<10^{-3}$). If this criterion (($f_{\gamma\gamma}/\delta^2$) = ($g_\gamma/\delta$) = $<10^{3}$)) is not met, δ is increased by $\Delta\delta$ and the boundary-layer equations are recomputed using the previously calculated profile functions as initial input. This process is repeated using an increased value of δ each time until the required edge condition ($<10^{-3}$) is met.

The usual differential calculation method assumes a δ, $\left(g_\gamma\right)_w$ and $\left(f_{\gamma\gamma}\right)_w$ and in one δ step iterates for the correct δ, $\left(g_\gamma\right)_w$, and $\left(f_{\gamma\gamma}\right)_w$ while simultaneously satisfying the edge boundary conditions $\left[\left(f_{\gamma\gamma}/\delta^2\right)_{\gamma=1.0} = \left(g_\gamma/\delta\right)_{\gamma=1.0} = <10^{-3}\right]$. This single δ step iteration system generally works very well except when the boundary-layer equations become very nonlinear (large β) for which the initial assumptions δ, $\left(g_\gamma\right)_w$ and $\left(f_{\gamma\gamma}\right)_w$ become very sensitive to the boundary-layer solution. Whereas, the present stepping-up-process calculation method completely eliminates the problem of assuming a good value for δ and also provides improved values of initial $\left(g_\gamma\right)_w$ and $\left(f_{\gamma\gamma}\right)_w$ as well as improved values of initial velocity and total enthalpy profiles for each new δ step. This initial-approximation difficulty is particularly accentuated for the large pressure gradient nozzle flows for which the momentum and energy equations become extremely nonlinear. The values of $\left(f_{\gamma\gamma}\right)_w$ and $\left(g_\gamma\right)_w$ can vary by orders of magnitude along the nozzle as shown by typical solutions of the boundary-layer equations tabulated in tables III to V.

Skin Friction, Heat-Transfer Parameters, and Boundary-Layer Thicknesses

The following definitions of various boundary-layer terms are useful for analyzing the behavior of the boundary layer as well as for comparison with experimental data and other theoretical analyses.

The total shear stress distribution across the boundary layer is defined as

$$\tau = (\mu + \rho\epsilon_m)\frac{\partial u}{\partial y} \tag{43}$$

Substituting the transformation equations (10), (30), and (32) in equation (43), the nondimensional shear-stress function becomes

$$\frac{\tau}{\frac{(\rho_0\mu_0)^{1/2}}{2\tilde{x}}u_e^{3/2}} = \mathscr{P}_f \tag{44}$$

From equation (44) the shear-stress function $\mathscr{P}_f$ is clearly shown to be the nondimensional shear-stress distribution across the boundary layer. At the wall the shear stress reduces to

$$\tau_w = \mu_w \left(\frac{\partial u}{\partial y}\right)_w = \frac{1}{2}\rho_e u_e^2 C_f \tag{45}$$

Substituting the transformation equations (10) into equation (45) and solving for the skin friction coefficient C_f gives

$$C_f = \frac{2}{\rho_e}\left(\frac{\rho_0\mu_0}{u_e 2\tilde{x}}\right)^{1/2}\left(Cf_{\eta\eta}\right)_w = \frac{2}{\rho_e}\left(\frac{\rho_0\mu_0}{u_e 2\tilde{x}}\right)^{1/2}\left(\mathscr{P}_f\right)_w \tag{46}$$

The total energy transfer in the boundary layer from equation (B19) (appendix B) can be expressed as

$$q = \left(\frac{\mu}{Pr_L} + \frac{\rho\epsilon_m}{Pr_T}\right)H_y + \mu\left(1 - \frac{1}{Pr_L}\right)\left(\frac{u^2}{2}\right)_y \tag{47}$$

At the wall the heat transfer reduces to

$$q_w = \frac{\mu_w}{Pr_L}\left(H_y\right)_w \tag{48}$$

Substituting the appropriate transformation equations (10), (30), and (33) in equation (48) gives for the heat transfer at the wall

$$q_w = \left(\frac{\rho_0\mu_0 u_e}{2\tilde{x}}\right)^{1/2} H_0\left(\mathscr{P}_g\right)_w \tag{49}$$

where $\left(\mathscr{P}_g\right)_w$ is the nondimensional heat-transfer function along the wall.

After substituting the proper transformation equations in equation (47), the ratio of the total (local) energy transfer to the wall heat transfer is obtained by dividing equation (47) by equation (49):

$$\frac{q}{q_w} = \frac{\mathscr{P}_g + 2D_3C\left(1 - \frac{1}{Pr_L}\right)f_\eta f_{\eta\eta}}{\left(\mathscr{P}_g\right)_w} \tag{50}$$

The total energy transfer across the boundary layer consists of the conduction heat transfer plus the total shear work. The total shear work is given by the following:

$$u\tau = \left(\frac{\rho_0 \mu_0 u_e}{2\tilde{x}}\right)^{1/2} H_0 2D_3 f_\eta \mathscr{P}_f \tag{51}$$

Dividing equation (51) by equation (49), the ratio of the total shear work to the wall heat transfer is

$$\frac{u\tau}{q_w} = \frac{2D_3 f_\eta \mathscr{P}_f}{\mathscr{P}_g} \tag{52}$$

From the definition of the total energy transfer ($q_T = q_c + u\tau$) the conduction heat transfer divided by the wall value is simply

$$\frac{q_c}{q_w} = \frac{q}{q_w} - \frac{u\tau}{q_w} \tag{53}$$

The usual heat-transfer coefficient based on enthalpy is given by

$$C_q = \frac{q_w}{(H_{aw} - H_w)} \tag{54}$$

where H_{aw}, the adiabatic wall enthalpy, is defined as

$$H_{aw} = h_e + r_c(H_0 - h_e) \tag{55}$$

and the recovery factor r_c is (as usually assumed)

$$r_c = (Pr_L)^{1/3} \tag{56}$$

The static enthalpy at the edge of the boundary layer h_e is

$$h_e = c_p t_e \tag{57}$$

Likewise, the wall enthalpy H_w with ($u = 0$) becomes

$$H_w = c_p T_w \tag{58}$$

For comparison with experimental measurements and other theoretical analyses, the following boundary-layer thicknesses are very useful:

Thickness	Definition	Transformed
Momentum	$\theta = \int_0^{y_\infty} \frac{\rho u}{\rho_e u_e}\left(1 - \frac{u}{u_e}\right) dy$	$\theta = \left(\frac{\rho_e \mu_0 2\bar{x}}{u_e}\right)^{1/2} \frac{1}{\rho_e} \int_0^{\eta_\infty} f_\eta (1 - f_\eta)\, d\eta$
Displacement	$\delta^* = \int_0^{y_\infty} \left(1 - \frac{\rho u}{\rho_e u_e}\right) dy$	$\delta^* = \left(\frac{\rho_0 \mu_0 2\bar{x}}{u_e}\right)^{1/2} \frac{1}{\rho_e} \int_0^{\eta_\infty} \left(\frac{1}{\rho/\rho_e} - f_\eta\right) dy$
Energy	$\phi = \int_0^{y_\infty} \frac{\rho u}{\rho_e u_e}\left(1 - \frac{T - T_w}{T_0 - T_w}\right) dy$	$\phi = \left(\frac{\rho_0 \mu_0 2\bar{x}}{u_e}\right)^{1/2} \frac{1}{\rho_e} \int_0^{\eta_\infty} f_\eta \left(1 - \frac{g - g_w}{1 - g_w}\right) d\eta$

COMPARISON OF PRESENT THEORY WITH EXPERIMENTAL MEASUREMENTS

The usual test of the accuracy of a theoretical boundary-layer analysis is a comparison of predicted results with exact solutions or experimental measurements. Because exact solutions for turbulent flow are not available, the numerical technique was first checked out with laminar flow calculations and compared favorably with references 13 and 14. The present turbulent boundary-layer analysis is compared with the Bartz turbulent, integral-boundary layer analysis (ref. 1) and experimental data of references 6 to 8 for a 30° half angle of convergence, and 15° half angle of divergence cooled nozzle with cooled and uncooled inlets. In references 6 to 8 the heat transfer and wall

temperature were measured at 20 nozzle locations from tests conducted in heated air at nominal stagnation pressures of 207 and 20.7 newtons per square centimeter (300 and 30 psia) and a nominal stagnation temperature of 539 K (970° R). Boundary-layer profiles were also measured at several locations along the nozzle, as indicated in table I. These nozzle measurements have been made for the following different inlet flow conditions:

(1) The uncooled inlet with the boundary layer bled off at the nozzle entrance

(2) The uncooled inlet with no boundary layer bleed

(3) The cooled inlet

(4) The cooled inlet at low pressure.

For this first inlet flow (uncooled inlet with bleed) the turbulent boundary layer starts at the nozzle entrance. For the second inlet flow (uncooled inlet without bleed), the turbulent boundary layer is assumed to begin 254 centimeters (1 in.) just inside the uncooled inlet (see table I). The third inlet flow (the cooled inlet) produces a thermal as well as a velocity turbulent boundary-layer history coming into the 30° nozzle. The nozzle data (refs. 6 to 8) for the first three inlet flows are taken from tests conducted with air at a nominal stagnation temperature of 539 K (970° R) and nominal stagnation pressure of 207 newtons per square centimeter (300 psia). The nozzle data for the last inlet flow condition (cooled inlet) are taken from tests conducted with air at a low stagnation pressure of 20.7 newtons per square centimeter (30 psia).

Heat Transfer

The measured wall temperatures along the nozzle are used as the boundary condition at the wall in the solution for the energy equation. Since the present turbulent Prandtl number correlation (eq. (26)) has been developed using the measured heat transfer along the nozzle with the uncooled inlet flow condition (without the boundary-layer bleed), only a heat-transfer comparison of the present theory with experimental data for the nozzle with the remaining different inlet flow conditions is meaningful.

In figures 2(a) and 3 the (present theory) prediction of the heat-transfer distribution along the nozzle with the previously discussed different inlet flow are compared with experimental data (refs. 6 to 8) and the turbulent integral boundary layer analysis of Bartz (ref. 1). Except for the low pressure case (fig. 3(b)), the (present theory) prediction is in excellent agreement with the measured heat-transfer data in the throat and supersonic regions of the nozzle (see figs. 2(a) and (3)). In the low subsonic flow region of the nozzle the present theory underpredicts the measured heat transfer for each inlet flow condition. The integral boundary-layer calculation of Bartz generally overpredicts the heat transfer in the throat region and underpredicts the heat transfer in the subsonic and supersonic regions of the nozzle (see figs. 2 and 3). For the cooled inlet flow case at low total pressure a laminar boundary-layer calculation (present calculation method)

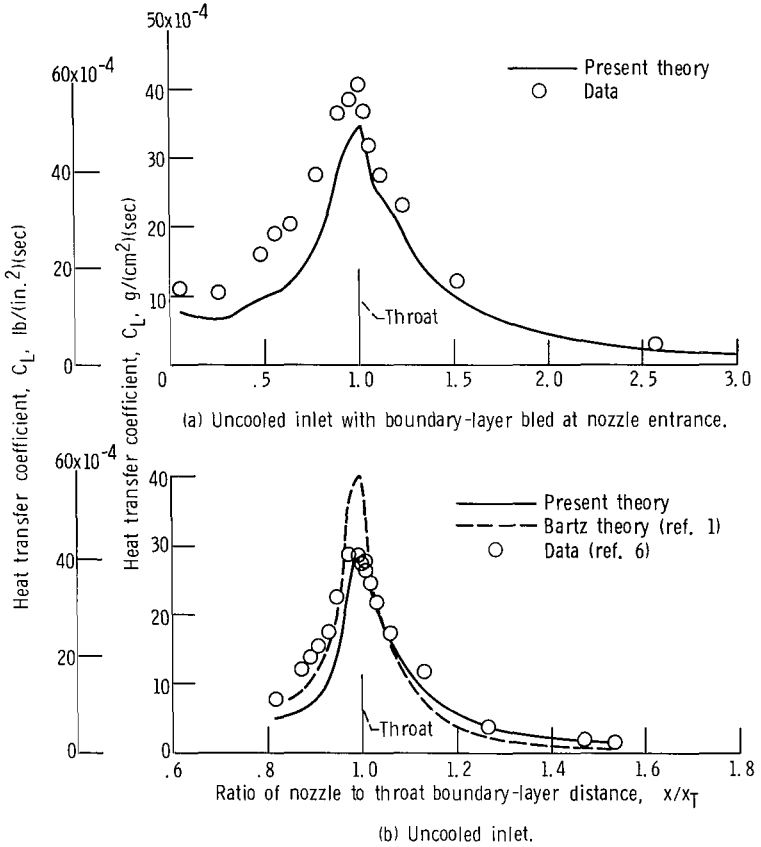

(a) Uncooled inlet with boundary-layer bled at nozzle entrance.

(b) Uncooled inlet.

Figure 2. - Predicted heat-transfer distributions in 30° nozzle with uncooled inlet and comparison with experimental data. Stagnation pressure, 207 newtons per square meter (300 psia).

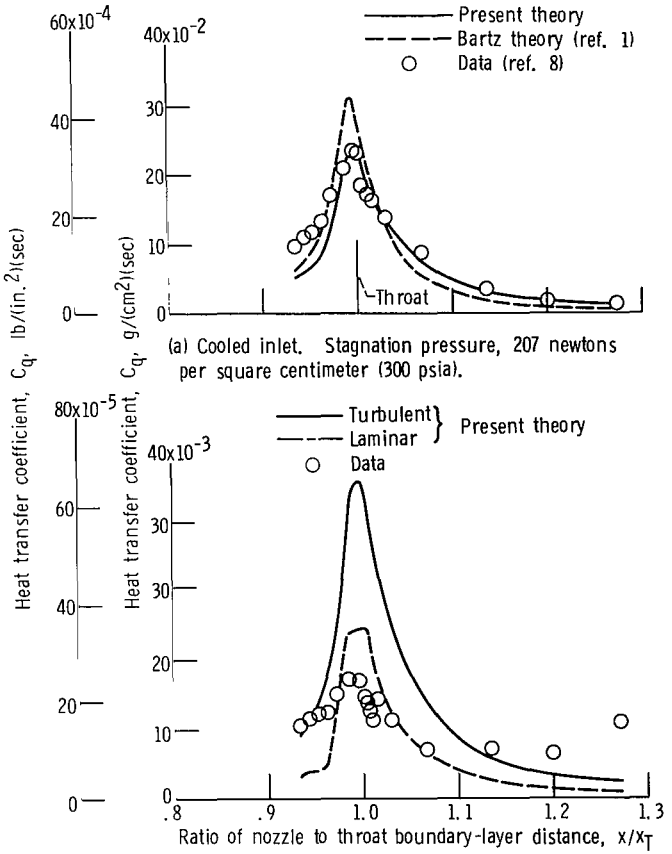

(a) Cooled inlet. Stagnation pressure, 207 newtons per square centimeter (300 psia).

(b) Cooled inlet. Stagnation pressure, 20.65 newtons per square centimeter (30 psia).

Figure 3. - Predicted heat-transfer distributions in 30° nozzle with cooled inlet and comparison with experimental data.

is also presented and compares more favorably with the measured nozzle heat transfer than the turbulent (present theory) heat transfer (see fig. 3(b)).

Boundary-Layer Profiles

A boundary-layer probing station is located in the uncooled inlet approach section just a few centimeters upstream of the conical nozzle (see ref. 6 for details). In figure 4 the predicted velocity profile as a function of the similarity transformation variation η is in excellent agreement with experimental data for this subsonic, zero pressure gradient, inlet pipe flow. In the supersonic flow region of the nozzle figures 5 to 8 show good agreement of the predicted velocity and total enthalpy profiles with experimental data at stations 18 and 19a (see table I) for the uncooled inlet flow condition. Both the predicted and experimental boundary-layer profiles are presented as a function of the similarity transformation variable η. Unlike Deissler's wall distance variable y^+ (ref. 9), this similarity variable η does not require a knowledge of the experimental skin friction coefficient.

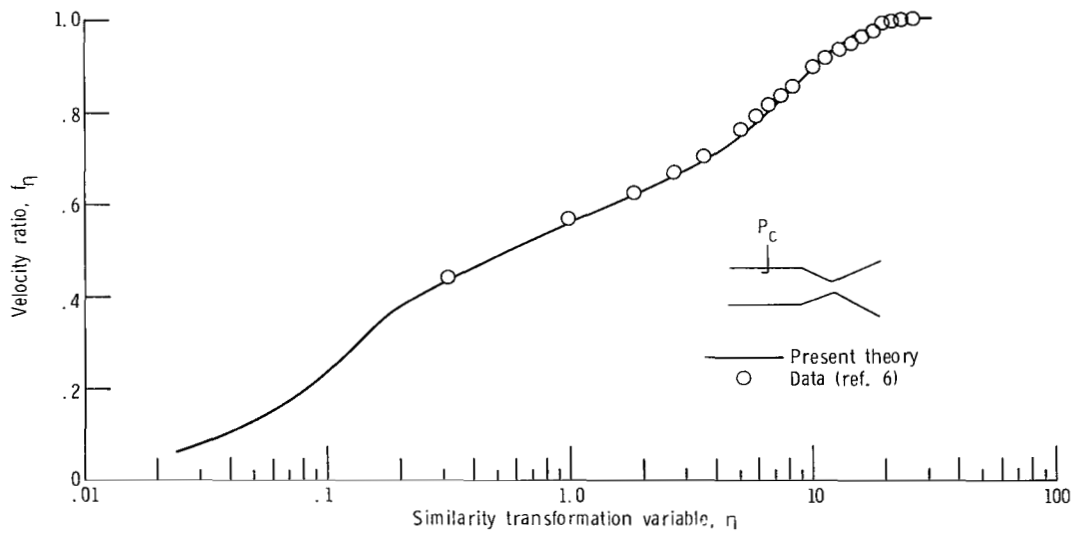

Figure 4. - Comparison of predicted velocity profile with experimental data at the uncooled cylindrical inlet probing station (P_c).

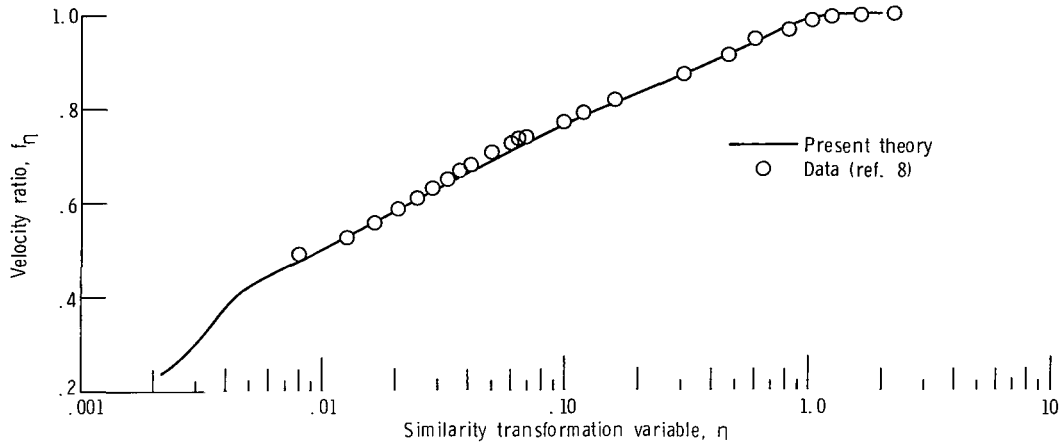

Figure 5. - Comparison of predicted velocity profile with experimental data at station 18 for 30° nozzle with uncooled inlet.

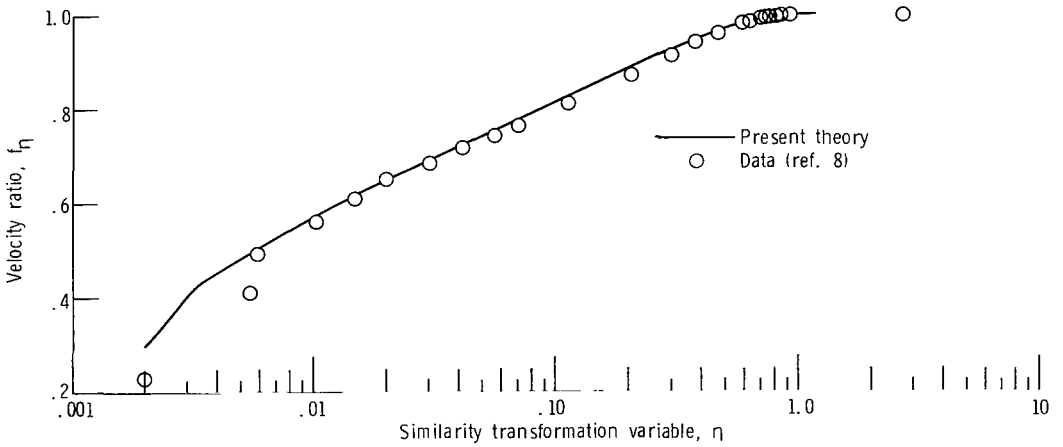

Figure 6. - Comparison of predicted velocity profile with experimental data at station 19a for 30° nozzle with uncooled inlet.

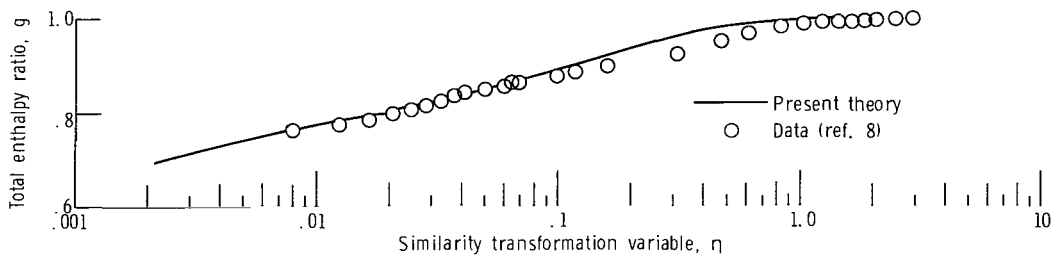

Figure 7. - Comparison of predicted total enthalpy profile with experimental data at station 18 for 30° nozzle with uncooled inlet (no boundary-layer bleed).

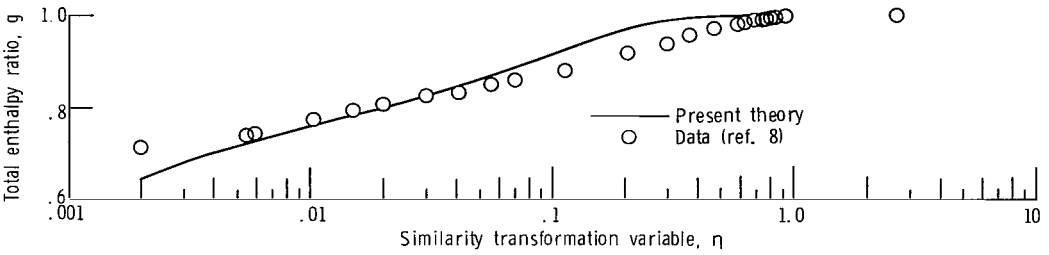

Figure 8. - Comparison of predicted total enthalpy profile with experimental data at station 19a for 30^0 nozzle with uncooled inlet (no boundary-layer bleed).

Boundary-Layer Thicknesses

In figures 9 to 11 the predicted momentum, displacement and energy thickness distributions along the nozzle for the four inlet flow conditions are compared with experimental data and the integral boundary-layer analysis of Bartz. In general, the predicted nozzle thicknesses (momentum, displacement, and energy) from both the Bartz and the present theory are in favorable agreement with the experimental nozzle data (see figs. 9 to 11). In figures 9(d), 10(d), and 11(d) a laminar as well as a turbulent (present theory) prediction of the nozzle thicknesses are presented for the cooled inlet flow condition at a pressure P_0 of approximately 20.7 newtons per square centimeter (30 psia).

INTREPRETATION OF NUMERICAL RESULTS

Boundary-Layer Input Quantities

Before analyzing the numerical results it is helpful to know what parameters and quantities (obtained from measurements or inviscid flow calculations) are given input to the boundary-layer calculations. The measured pressure ratios along the nozzle are used to calculate the velocity gradient parameter β; likewise, the nozzle geometry R is calculated from the nozzle coordinates (see fig. 12). If measured pressure ratios are not available, a one-dimensional isentropic flow assumption can be used to approximate the pressure ratios. An estimation of the turbulent boundary length upstream of the nozzle entrance is needed in order to determine the turbulent, boundary-layer, distance coordinate x as an input quantity along the nozzle (see fig. 1). Since the turbulent Prandtl number Pr_T is assumed to be a constant across the boundary layer, it can be considered as an input quantity to the boundary-layer calculation. From figure 13 the Pr_T correlation has a strong streamwise nozzle variation with a large peak value slightly beyond the throat. These nozzle flow parameters as well as the turbulent Prandtl number are tabulated in tables VI to X for the 20 heat-transfer measuring sta-

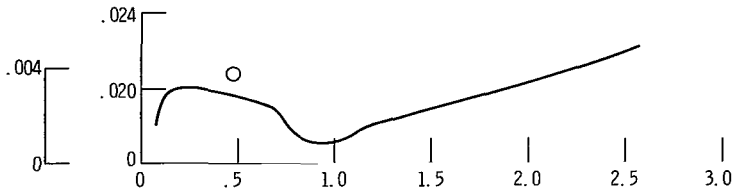

(a) Uncooled inlet with boundary-layer bleed at nozzle entrance. Stagnation pressure, 207 newtons per square centimeter (300 psia).

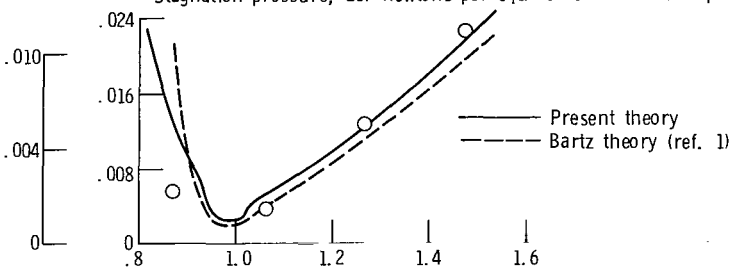

(b) Uncooled inlet. Stagnation pressure, 207 newtons per square centimeter (300 psia).

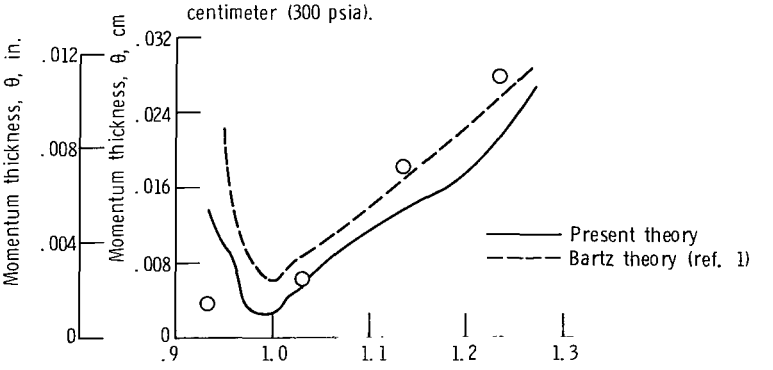

(c) Cooled inlet. Stagnation pressure, 207 newtons per square centimeter (300 psia).

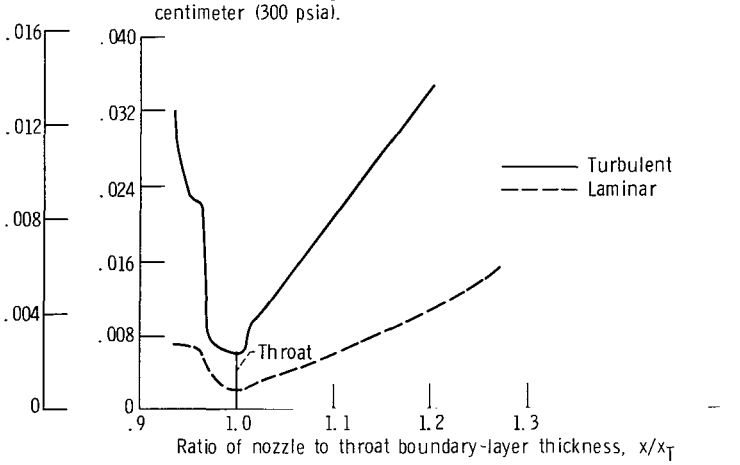

(d) Cooled inlet. Stagnation pressure, 20.65 newtons per square centimeter (30 psia).

Figure 9. - Variation of predicted momentum thickness along 30^0 nozzle with cooled and uncooled inlets and comparison with experimental data (ref. 6 to 8).

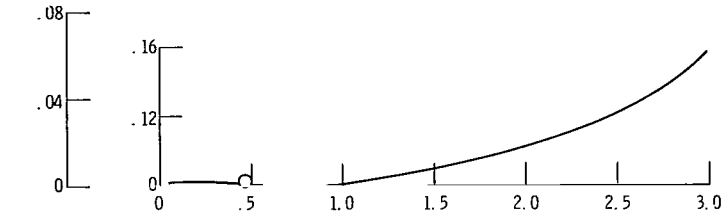

(a) Uncooled inlet with boundary-layer bleed at nozzle entrance. Stagnation pressure, 207 newtons per square centimeter (300 psia).

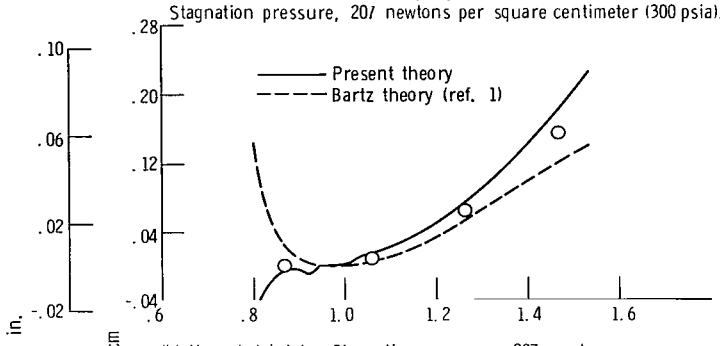

(b) Uncooled inlet. Stagnation pressure, 207 newtons per square centimeter (300 psia).

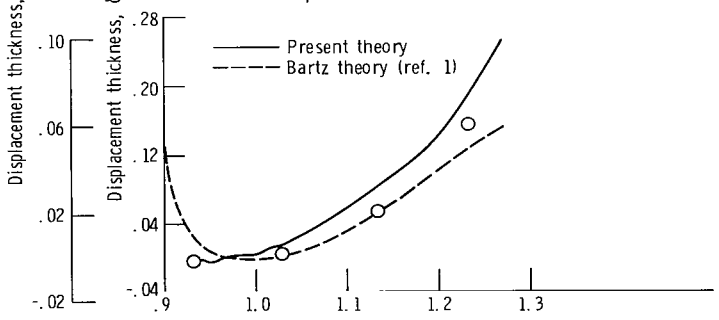

(c) Cooled inlet. Stagnation pressure, 207 newtons per square centimeter (300 psia).

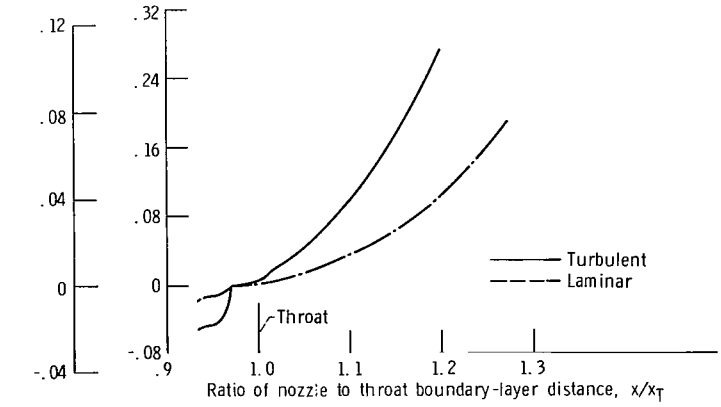

(d) Cooled inlet. Stagnation pressure, 20.65 newtons per square centimeter (30 psia).

Figure 10. - Variation of predicted displacement thickness along 30^0 nozzle with cooled and uncooled inlets and comparison with experimental data (refs. 6 to 8).

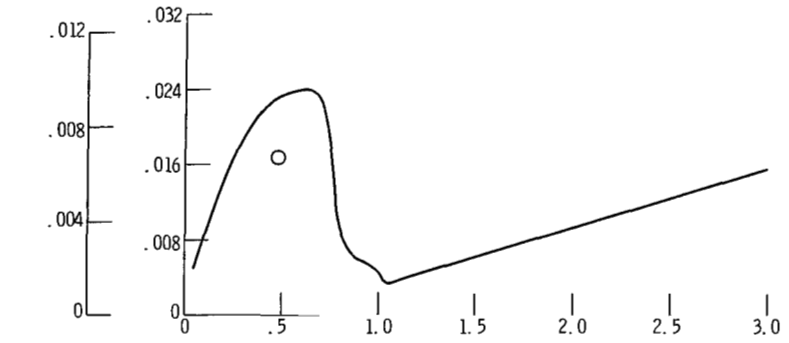

(a) Uncooled inlet with boundary-layer bleed at nozzle entrance. Stagnation pressure, 207 newtons per square centimeter (300 psia).

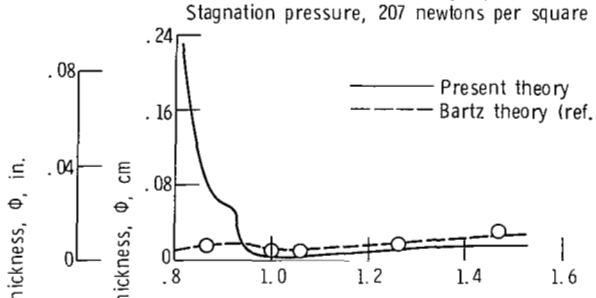

(b) Uncooled inlet. Stagnation pressure, 207 newtons per square centimeter (300 psia).

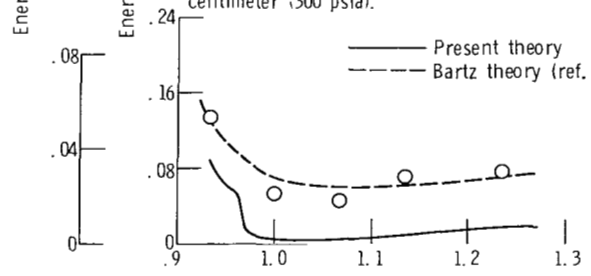

(c) Cooled inlet. Stagnation pressure, 207 newtons per square centimeter (300 psia).

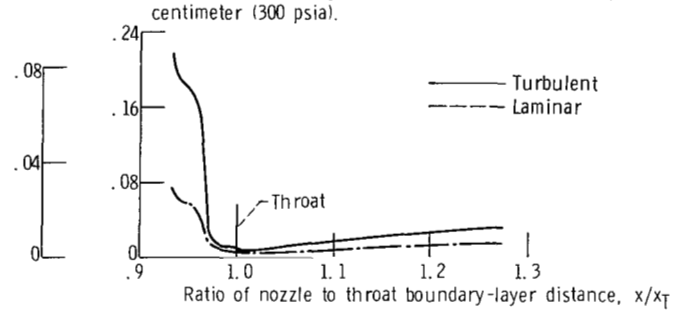

(d) Cooled inlet. Stagnation pressure, 20.65 newtons per square centimeter (30 psia).

Figure 11. - Variation of predicted energy thickness along 30^0 nozzle data cooled and uncooled inlets and comparison with experimental data (refs. 6 to 8).

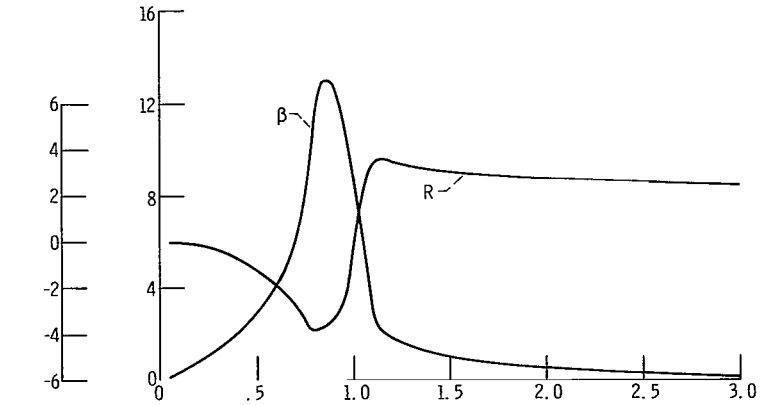

(a) Uncooled inlet with boundary-layer bleed at nozzle entrance.

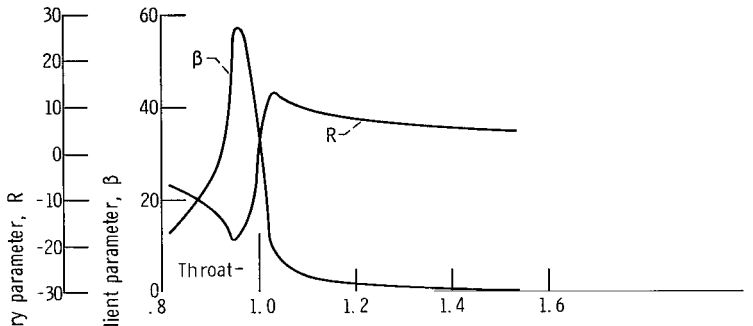

(b) Uncooled inlet.

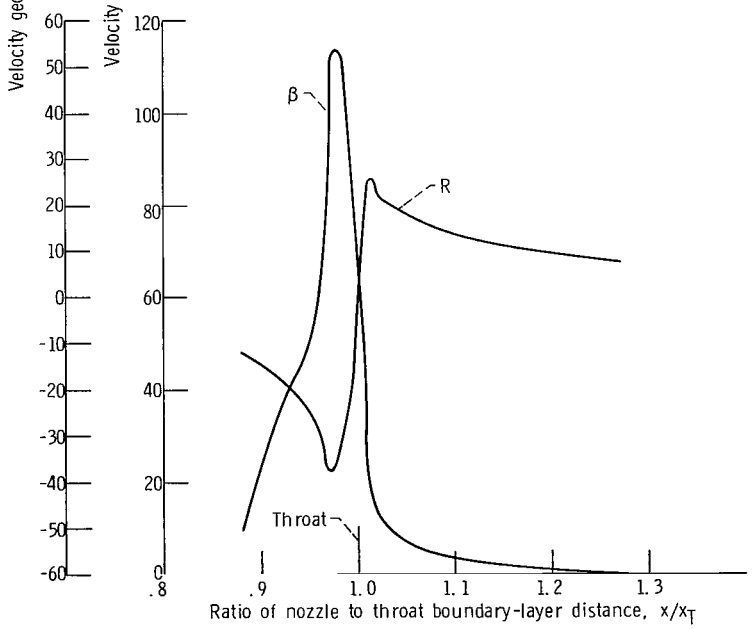

(c) Cooled inlet.

Figure 12. - Variation of velocity gradient and nozzle geometry parameters along 30° nozzle with uncooled and cooled inlets.

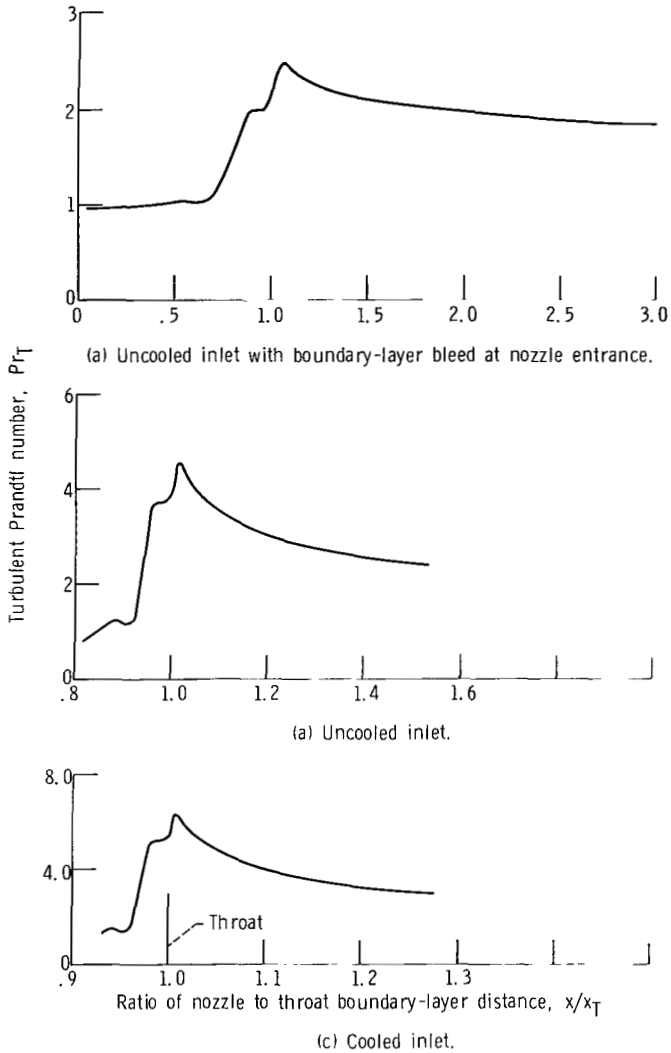

Figure 13. - Variation of correlated turbulent Prandtl number along 30° nozzle for uncooled and cooled inlets.

tions along the nozzle. As previously mentioned the measured wall temperatures along the nozzle are used as the boundary condition at the wall in the solution for the energy equation.

Effect of the Velocity Gradient Parameter

The velocity gradient parameter β has a very strong effect on the accelerated, boundary-layer, nozzle flow. In fact, the velocity gradient parameter appears to control the level and variation of the wall shear-stress function, $\left(\mathscr{P}_f\right)_w$, along the nozzle (see

fig. 14). The shape of $\left(\mathscr{P}_f\right)_w$ is very similar to β even to its peak value occurring at about the same nozzle station as the maximum β, slightly upstream of the throat. This wall shear stress function $\left(\mathscr{P}_f\right)_w$ is very important since $\left(\mathscr{P}_f\right)_w$ is the variation of the nondimensional wall shear-stress along the nozzle (see eq. (44)).

At first, large β was thought to be the sole factor in dominating the momentum boundary layer by means of the large pressure gradient term

$$\delta^3\beta\left[\frac{1}{\rho/\rho_e}-\left(\frac{f_\gamma}{\delta}\right)^2\right]$$

the right side of momentum equation (34). But, since the inner bracketed part

$$\left[\frac{1}{\rho/\rho_e}-\left(\frac{f_\gamma}{\delta}\right)^2\right]$$

of the pressure gradient term is generally a maximum (slightly less than one) and fairly constant along the wall, the value of $\delta^3\beta$ (which is very large) and not just β will control the acceleration effect on the momentum boundary layer. Remember that δ is the boundary-layer thickness in the transformed η coordinate and will strongly depend on the upstream boundary-layer history. From figure 15(a) $\delta^3\beta$ is a maximum at about station 7 ($x/x_T = 0.7021$) in the nozzle for the uncooled inlet with the boundary layer bled off at the nozzle entrance. In figure 15(b) $\delta^3\beta$ has two peak values along the nozzle for the uncooled inlet. The first and largest peak value of $\delta^3\beta$ occurs at station 3 ($x/x_T = 0.8139$) and the second peak value occurs at station 9 ($x/x_T = 0.9701$). This same behavior of two peak values of $\delta^3\beta$ at approximately the same nozzle locations is also present for the cooled inlet case (see fig. 15(c)). The first peak value of $\delta^3\beta$ is a result of the combination of a much larger β (than the case where the boundary layer is bled off at the nozzle entrance) and only a slightly smaller δ since a large β tends to reduce the increased δ (due to the upstream inlet boundary layer). The second peak value of $\delta^3\beta$, as one might suspect, occurs at the maximum value of β (station 9) in the nozzle for both the cooled and uncooled inlets. Therefore, the greatest acceleration effects on the momentum boundary layer in the nozzle are expected to occur in these two peak regions of $\delta^3\beta$. Some justification of this is evident from figures 16 and 17 which show that the skin friction coefficient maximizes at the same location as the first peak in $\delta^3\beta$ (station 3).

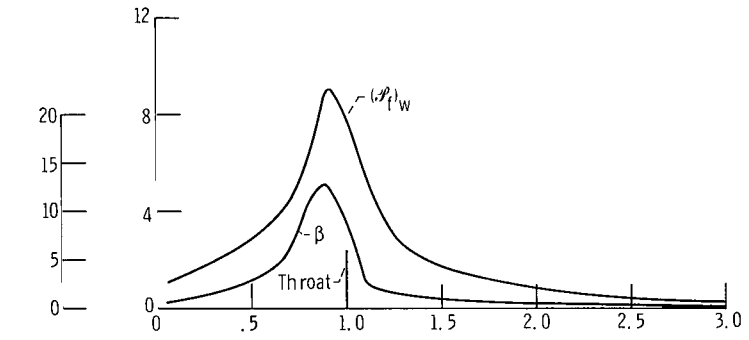

(a) Uncooled inlet with boundary-layer bleed at nozzle entrance.

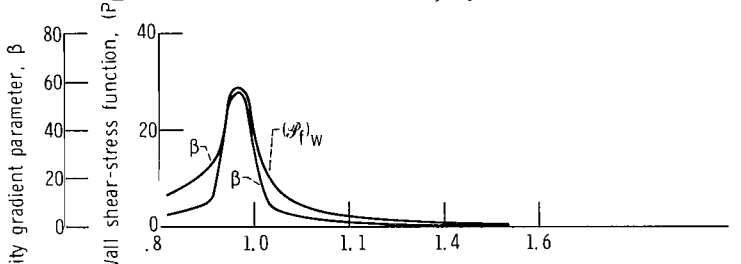

(b) Uncooled inlet.

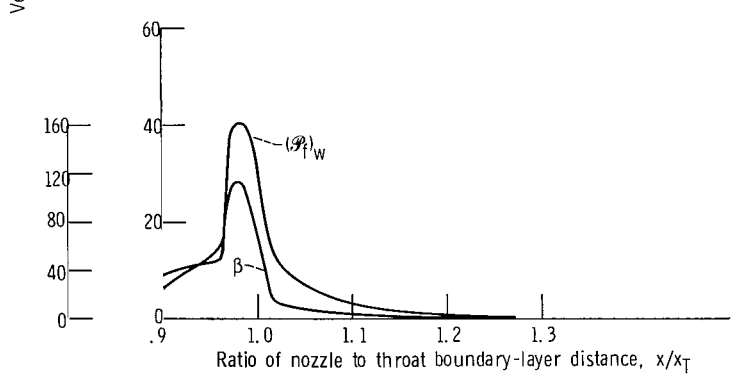

(c) Cooled inlet.

Figure 14. - Variation of wall shear stress function and velocity gradient parameter along the nozzle for uncooled and cooled inlets. Stagnation pressure, 207 newtons per square centimeter (300 psia).

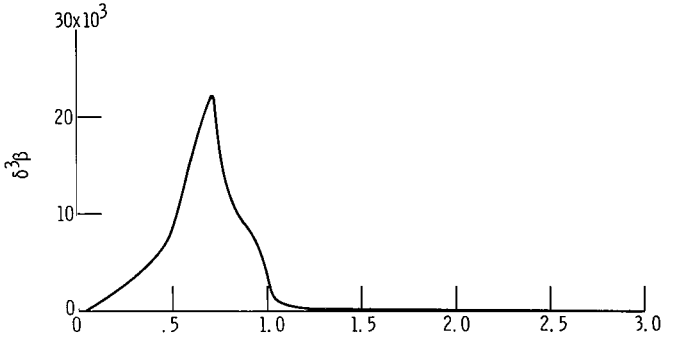

(a) Uncooled inlet with boundary-layer bleed at nozzle entrance.

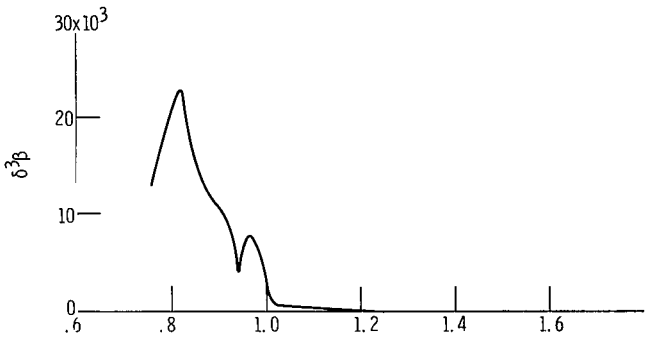

(b) Uncooled inlet.

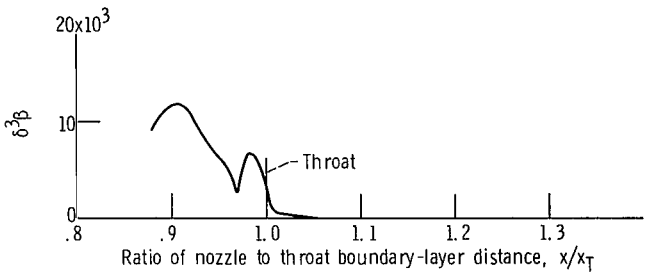

(c) Cooled inlet.

Figure 15. - Variation of $\delta^3\beta$ along nozzle for uncooled and cooled inlets. Stagnation pressure, 207 newtons per square centimeter (300 psia).

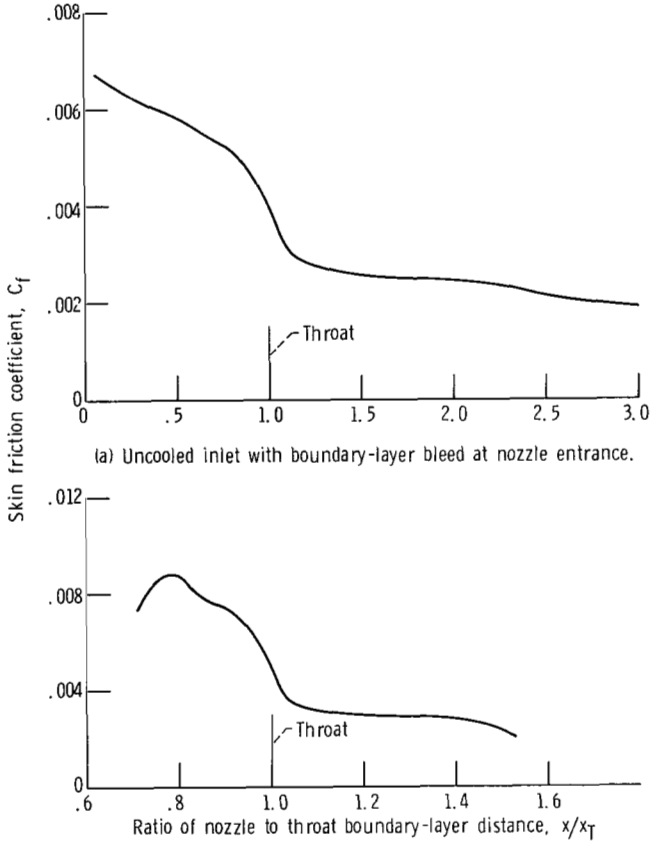

(a) Uncooled inlet with boundary-layer bleed at nozzle entrance.

(b) Uncooled inlet.

Figure 16. - Predicted skin friction coefficient distributions in 30° nozzle with uncooled inlet. Stagnation pressure, 207 newtons per square centimeter (300 psia).

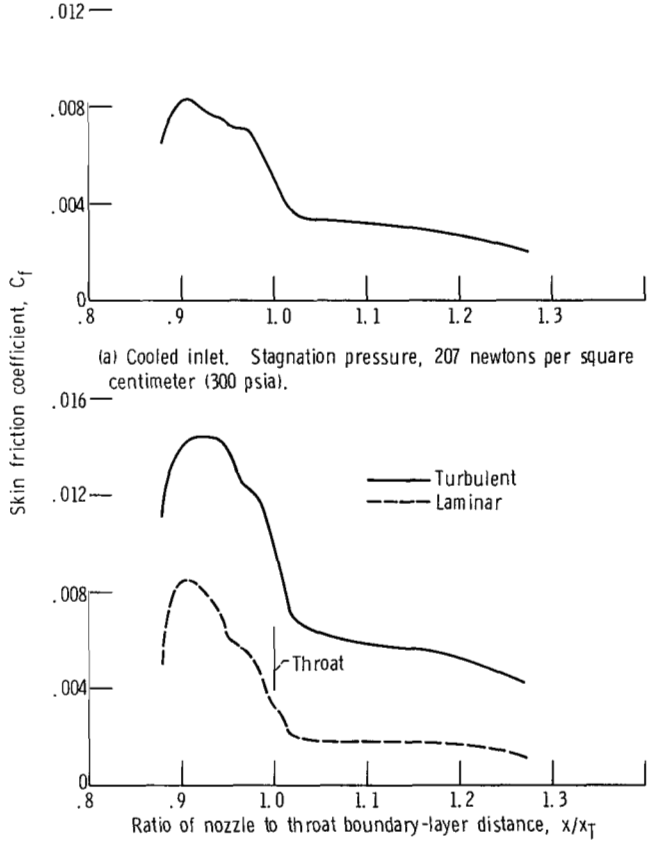

(a) Cooled inlet. Stagnation pressure, 207 newtons per square centimeter (300 psia).

(b) Cooled inlet. Stagnation pressure, 20.65 newtons per square centimeter (30 psia).

Figure 17. - Predicted skin friction coefficient distributions in 30° nozzle with cooled inlet.

Effect of the Turbulent Prandtl Number

A constant Pr_T of one throughout the 30^o nozzle was first used in the boundary-layer equations. This calculation grossly overpredicted the heat transfer in the throat and supersonic regions of the nozzle. In fact, these predicted heat-transfer results are more typical of the usual Nusselt number heat-transfer correlation in the throat region (see ref. 7). From this heat-transfer comparison, it is readily apparent that a much larger Pr_T than one is necessary for a good heat-transfer comparison of the present prediction with data. At first, this requirement ($Pr_T >> 1.0$) seems unusual, but Bushnell and Beckwith (ref. 5) have shown with their finite-difference, numerical, turbulent boundary-layer calculation that $Pr_T \geq 1.5$ are necessary for good agreement with data in the throat and supersonic region. This requirement of large Pr_T is believed to result from the fact that the present theory and reference 5 use a Pr_T which is based on the total enthalpy gradient and not the usual static enthalpy (temperature) gradient.

From purely trial and error and numerical experience, a turbulent Prandtl number correlation (eq. (26)) has been developed using the experimental data from the 30^o nozzle with the uncooled inlet flow condition (ref. 7). This Pr_T, which is a constant across the boundary layer, varies from approximately one in the nozzle entrance region to a large peak value in the throat region and still remains a large value in the supersonic region (see fig. 13). Also, from figure 13 the variation of Pr_T along the nozzle is readily seen to change as the inlet flow condition is changed.

In order to test this Pr_T correlation, the present theory has been applied to the 30^o nozzle with the cooled inlet flow condition. From figure 4(a) the predicted heat transfer is shown to be in excellent agreement with the experimental heat transfer in the throat and supersonic region of the nozzle with this cooled inlet flow condition. In addition, the present analysis has also been applied to a 45^o angle of convergence 15^o angle of divergence nozzle (ref. 15) with a total temperature T_0 of 1110 K (2000^o R) and a total pressure P_0 of 103.5 newtons per square centimeter (150 psi). The predicted heat transfer agreed within 9 percent of the experimental 45^o nozzle heat-transfer data in the throat region.

Possibly from a lesser point of interest than Pr_T, the total energy transfer across the boundary layer has been expressed in terms of its components: the conduction heat transfer and the shear work. Figure 18 shows the variation of the total energy transfer, the conduction heat transfer and the shear work (all referenced to the wall heat transfer) across the turbulent boundary layer for station 9, 11 (throat), and 20 (nozzle exit) along the 30^o nozzle with the cooled inlet. It is interesting to note the growing importance of the large shear work term proceeding from the throat to the supersonic nozzle exit region.

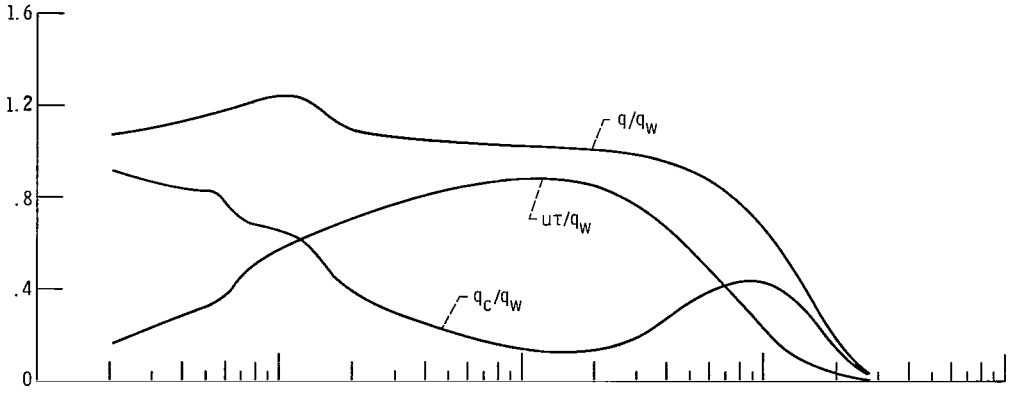

(a) Station 9; ratio of nozzle to throat boundary layer distance, 0.9849.

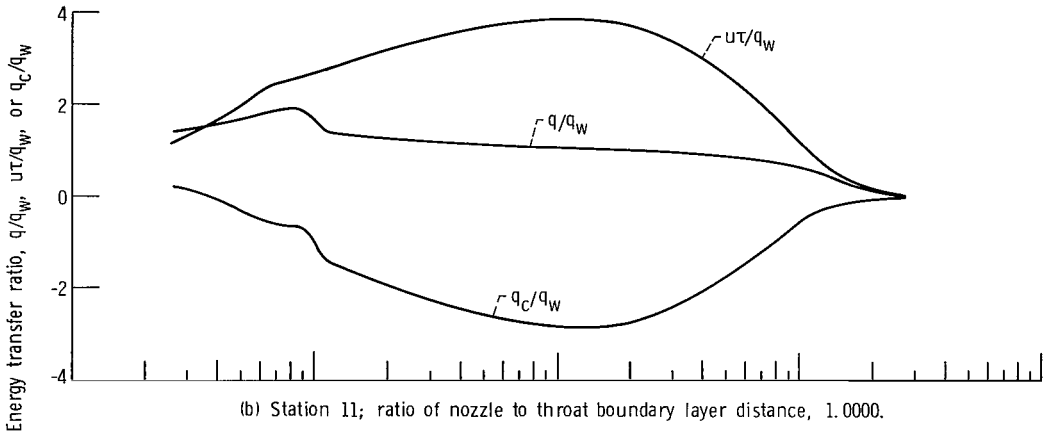

(b) Station 11; ratio of nozzle to throat boundary layer distance, 1.0000.

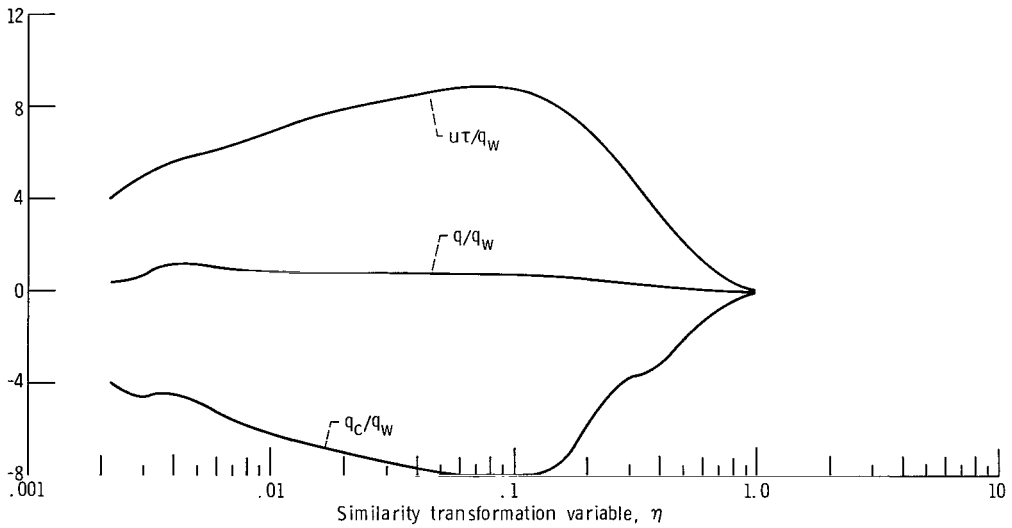

(c) Station 20; ratio of nozzle to throat boundary layer distance, 1.272.

Figure 18. - Variation of total energy transfer, conduction heat transfer, and shear work (q/q_w, q_c/q_w, and $u\tau/q_w$) across boundary layer for several stations along 30^0 nozzle with cooled inlet.

CONCLUDING REMARKS

A similar-solution differential turbulent boundary-layer analysis has been developed in order to provide a relatively simple heat-transfer prediction along a nozzle. This analysis along with a new correlation for the turbulent Prandtl number gives good agreement of the predicted with the measured heat transfer in the throat and supersonic region of a nozzle. Also, the turbulent boundary-layer variables (heat transfer, etc.) can be calculated at any arbitrary location in the throat of supersonic region of the nozzle in less than a half minute of computing time (Lewis DCS 7094-7044). For example, the boundary layer at the nozzle exit location can be calculated directly without the requirement of the usual step-by-step marching-calculation method for the complete nozzle boundary layer.

Lewis Research Center,
National Aeronautics and Space Administration,
Cleveland, Ohio, April 20, 1971,
120-27.

APPENDIX A

SYMBOLS

A_E flow coefficient, eq. (40)

A_M flow coefficient, eq. (38)

B_E flow coefficient, eq. (41)

B_M flow coefficient, eq. (39)

C density-viscosity ratio, eq. (13)

C_f skin friction coefficient

C_q heat-transfer coefficient

$\overline{C}_1$ transformation parameter, eq. (32)

$\overline{C}_2$ transformation parameter, eq. (33)

c_p specific heat at constant pressure

D nozzle diameter

D_1 flow coefficient, eq. (17)

D_2 flow coefficient, eq. (18)

D_3 flow coefficient, eq. (15)

$\frac{du_e}{dx}$ velocity derivative at edge of boundary layer

e natural or Naperian base ($e = 2.71828$)

f_η velocity ratio, u/u_e

g total enthalpy ratio, H/H_0

H total enthalpy

h static enthalpy

K_1 constant of integration, eq. (C18)

K_2 constant of integration ($K_2 = 0$)

K_3 constant of integration ($K_3 = 0$)

K_4 constant of integration, eq. (C24)

K_5 constant of integration ($K_5 = g_w$)

M Mach number

n empirical constant (0.109)

P static pressure

$\mathscr{P}_f$ dependent variable transformation, eq. (30)

$\mathscr{P}_g$ dependent variable transformation, eq. (31)

Pr_L laminar Prandtl number

Pr_T turbulent Prandtl number (based on total enthalpy gradient)

q total energy transfer through boundary layer

q_c conduction heat transfer through the boundary layer

q_w wall heat transfer

R nozzle geometry parameter

$\mathscr{R}$ universal gas constant

r nozzle radius

r_c recovery factor

T total temperature

t static temperature

u velocity parallel to nozzle surface

$\overline{u'v'}$ fluctuating velocity, double-correlation term

v velocity normal to nozzle surface

$\overline{v'H'}$ fluctuation, velocity-total enthalpy, double-correlation term

$\overline{v'h'}$	fluctuating, velocity-static enthalpy, double-correlation term
$\tilde{x} = x$	coordinate parallel to nozzle surface
y	coordinate normal to nozzle surface
y^+	wall distance parameter, eq. (24)
z	axial distance along nozzle
β	velocity gradient parameter, eq. (19)
γ	transformed coordinate, eq. (27)
δ	boundary layer thickness in η coordinate
δ^*	compressible displacement thickness
δ_i^*	incompressible displacement thickness
ϵ_H	eddy diffusivity for heat transfer based on total enthalpy gradient
ϵ_m	momentum eddy diffusivity
$\epsilon_{m,1}$	momentum eddy diffusivity for laminar sublayer region
$\epsilon_{m,2}$	momentum eddy diffusivity for law of the wall region
$\epsilon_{m,3}$	momentum eddy diffusivity for outer intermittency region
η	transformed similarity coordinate in y-direction
θ	momentum thickness
κ	empirical constant (0.40)
μ	molecular viscosity
ζ	empirical constant (0.018)
ρ	density
τ	total shear stress distribution across the boundary layer
τ_w	wall shear stress
ϕ	energy thickness
ψ	stream function
ω_m	integration factor, eq. (C17)
ω_ϵ	integration factor, eq. (C23)

Superscripts:

d	exponent for viscosity variation with temperature (0.65 for air)
-	average value of variable
'	fluctuation value of variable

Subscripts:

aw	adiabatic wall condition
e	edge of boundary-layer conditions
w	wall conditions
y, yy, or x, xx	indicates derivatives of function with respect to y- or x-coordinate
$\eta, \eta\eta$ or $\gamma, \gamma\gamma$	indicates derivatives of function with respect to the η- or γ-coordinate
0	stagnation conditions

APPENDIX B

DEVELOPMENT OF THE TURBULENT, COMPRESSIBLE, BOUNDARY-LAYER EQUATIONS

The boundary-layer equations for axisymmetric steady flow neglecting surface curvature and assuming constant pressure across the boundary layer are (ref. 16):

Continuity

$$(r\rho u)_x + (r\rho v)_y = 0 \tag{B1}$$

Momentum

$$\rho u(u)_x + \rho v(u)_y = -(P)_x + (\mu u_y)_y \tag{B2}$$

Energy

$$\rho u(h)_x + \rho v(h)_y = u(P)_x + \left(\frac{\mu}{Pr_L} h_y\right)_y + \mu(u_y)^2 \tag{B3}$$

State

$$P = \rho \mathscr{R} T \tag{B4}$$

(Symbols are defined in appendix A.)

The momentum equation can be rearranged as follows. Multiplying equation (B1) by u and equation (B2) by r, and adding the resulting equations gives

$$(r\rho u^2)_x + (r\rho uv)_y = -r(P)_x + r\left[\mu u_y\right]_y \tag{B5}$$

The energy equation can be similarly rearranged. Multiplying equation (B1) by h and equation (B3) by r, and adding the resulting equations gives

$$(r\rho uh)_x + (r\rho vh)_y = ru(P)_x + r\left(\frac{\mu}{Pr_L} h_y\right)_y + r\mu(u_y)^2 \tag{B6}$$

Now, by denoting the average and fluctuating values of variables as

$$\left.\begin{aligned} u &= \bar{u} + u' \\ P &= \bar{P} + P' \\ v &= \bar{v} + v' \\ h &= \bar{h} + h' \\ H &= \bar{\bar{H}} + H' \end{aligned}\right\} \tag{B7}$$

Note that fluctuating densities ρ' are neglected.

Substituting the first three expressions of equation (B7) into equation (B5) and using the continuity equation (B1) the momentum equation (after time averaging) becomes

$$\rho\bar{u}(\bar{u})_x + \rho\bar{v}(\bar{u})_y = -(P)_x + \left(\mu\bar{u}_y - \rho\overline{u'v'}\right)_y - r(\rho r\bar{u}'^2)_x \tag{B8}$$

Since the boundary layer is assumed to be thin, the term $-1/r\,(\rho r\overline{u'^2})_x$ is small compared with $-(\rho\overline{u'v'})_y$ and thereby neglected. The momentum equation now becomes

$$\rho\bar{u}(\bar{u})_x + \rho\bar{v}(\bar{u})_y = -(P)_x^+ + \left(\mu\bar{u}_y - \rho\overline{u'v'}\right)_y \tag{B9}$$

Similarly, substituting the expressions of equation (B7) into the energy equation (B6) and using the continuity equation (B1), the energy equation (after time averaging) becomes

$$\left[r\rho(\overline{uh} + \overline{u'h'})\right]_x + \left[r\rho(\overline{vh} + \overline{v'h'})\right]_y = r\mu\left(\frac{\partial\bar{u}}{\partial y}\right)^2 + r\left[\bar{u}\frac{d\bar{P}}{dx} + \overline{u'\left(\frac{dP}{dx}\right)'}\right]$$

$$+ r\frac{\partial}{\partial y}\left(\frac{\mu}{Pr_L}\frac{\partial\bar{h}}{\partial y}\right) + r\mu\overline{\left(\frac{\partial u}{\partial y}\right)'\left(\frac{\partial u}{\partial y}\right)'} \tag{B10}$$

The pressure gradient term in the energy equation (B10)

$$r\left[\bar{u}\frac{d\bar{P}}{dx} + \overline{u'\left(\frac{dP}{dx}\right)'}\right]$$

can be eliminated by multiplying the momentum equation (B5) by u, performing the time averaging process, using the time averaged continuity equation, and finally adding the resulting equation to equation (B10). After performing these operations and neglecting triple correlation terms, the resulting energy equation is

$$\rho\bar{u}\left(\bar{h}+\frac{\bar{u}^2}{2}\right)_x+\rho\bar{v}\left(\bar{h}+\frac{\bar{u}^2}{2}\right)_y=\left[\frac{\mu}{Pr_L}\bar{h}_y\right]_y-\frac{1}{r}\left[r\rho\left(\overline{u'h'}+\frac{3}{2}\bar{u}\,\overline{u'^2}\right)\right]_x$$

$$-\left[\rho\left(\overline{v'h'}+\bar{v}\frac{\overline{u'^2}}{2}+\bar{u}\,\overline{u'v'}\right)\right]_y+\mu(\bar{u})_y^2+\mu\overline{\left(\frac{\partial u}{\partial y}\right)'\left(\frac{\partial u}{\partial y}\right)'}+\overline{u(\mu\bar{u}_y)}_y \qquad \text{(B11)}$$

But

$$\overline{u\left[\mu\bar{u}_y\right]}_y=\left[\mu\left(\frac{u^2}{2}+\frac{\overline{u'^2}}{2}\right)_y\right]_y-\mu\overline{\left(\frac{\partial u}{\partial y}\right)'\left(\frac{\partial u}{\partial y}\right)'} \qquad \text{(B12)}$$

Since the boundary layer is assumed to be thin, the term $-\frac{1}{r}\left[r\rho\left(\overline{u'h'}+\frac{3}{2}\bar{u}\,\overline{u'^2}\right)\right]_x$ is small compared with $-\left[\rho\left(\overline{v'h'}+\bar{v}\frac{\overline{u'^2}}{2}+\bar{u}\,\overline{u'v'}\right)\right]_y$ and thereby neglected. Also, with the substitution of equation (B12) in the energy equation (B11), the energy equation becomes

$$\rho\bar{u}\left(\bar{h}+\frac{\bar{u}^2}{2}\right)_x+\rho\bar{v}\left(\bar{h}+\frac{\bar{u}^2}{2}\right)_y=\left[\frac{\mu}{Pr_L}\bar{h}_y\right]_y-\left[\rho\left(\overline{v'h'}+\bar{u}\,\overline{u'v'}+\bar{v}\frac{\overline{u'^2}}{2}\right)\right]_y+\left[\mu\left(\frac{\bar{u}^2}{2}\right)_y\right]_y \qquad \text{(B13)}$$

Expressing the energy equation (B13) in terms of the averaged total energy ($\bar{H}=\bar{h}+\bar{u}^2/2$) and fluctuating total energy term ($\overline{v'H'}$) gives

$$\rho\bar{u}(\bar{H})_x+\rho\bar{v}(\bar{H})_y=\left[\frac{\mu}{Pr_L}\bar{H}_y\right]_y-(\rho\overline{v'H'})_y+\left[\mu\left(1-\frac{1}{Pr_L}\right)\left(\frac{\bar{u}^2}{2}\right)_y\right]_y \qquad \text{(B14)}$$

where the fluctuating total energy term ($\overline{v'H'}$), neglecting triple correlation terms, exactly reduces to

$$\overline{v'H'} = \overline{v'h'} + \bar{u}\,\overline{u'v'} + \bar{v}\,\frac{\overline{u'^2}}{2} \tag{B15}$$

Using the concept of an eddy diffusivity, the double correlation terms ($\overline{u'v'}$ and $\overline{v'H'}$) can be written as

$$\overline{u'v'} = -\epsilon_m(\bar{u})_y \tag{B16}$$

$$\overline{v'H'} = -\epsilon_H(\bar{H})_y \tag{B17}$$

where ϵ_m and ϵ_H are respectively the eddy diffusivities for momentum and heat transfer. Note that the eddy diffusivity for heat transfer is based on total enthalpy.

The turbulent Prandtl number Pr_T based on total enthalpy is defined as

$$Pr_T = \frac{\epsilon_m}{\epsilon_H} = \frac{\overline{u'v'}}{\overline{v'H'}}\,\frac{(\bar{H})_y}{(\bar{u})_y} \tag{B18}$$

Substituting equations (B16) to (B17) in equation (B14), the energy equation becomes

$$\rho u(H)_x + \rho v(H)_y = \left[\left(\frac{\mu}{Pr_L} + \frac{\rho\epsilon_m}{Pr_T}\right)H_y\right]_y + \left[\mu\left(1 - \frac{1}{Pr_L}\right)\left(\frac{u^2}{2}\right)_y\right]_y \tag{B19}$$

Note that the bars ($\bar{u}$ $\bar{H}$) denoting averaged quantities are now omitted for all further equation development.

Substituting the concept of the eddy diffusivity for the turbulent shear stress (eq. (B16)) in equation (B9), the momentum equation becomes

$$\rho u(u)_x + \rho v(u)_y = -(P)_x + \left[(\mu + \rho\epsilon_m)u_y\right]_y \tag{B20}$$

By making the usual boundary layer assumption that the static pressure across the boundary layer is constant (P = Pe), the pressure gradient term in the above momentum equation (B20) reduces to:

$$(P)_x = -\rho_e u_e\left(u_e\right)_x \tag{B21}$$

With the substitution of equation (B21) in equation (B20), the momentum equation becomes

$$\rho u(u)_x + \rho v(u)_y = \rho_e u_e \left(u_e\right)_x + \left[(\mu + \rho\epsilon_m)u_y\right]_y \tag{B22}$$

Finally, including the continuity equation, the following system of compressible turbulent boundary-layer equations for axisymmetric steady flows can be expressed as

Continuity

$$(\rho ur)_x + (\rho vr)_y = 0 \tag{B23}$$

Momentum

$$\rho u(u)_x + \rho v(u)_y = + \rho_e u_e \left(u_e\right)_x + \left[(\mu + \rho\epsilon_m)u_y\right]_y \tag{B24}$$

Energy

$$\rho u(H)_x + \rho v(H)_y = \left[\left(\frac{\mu}{Pr_L} + \frac{\rho\epsilon_m}{Pr_T}\right)H_y\right]_y + \left[\mu\left(1 - \frac{1}{Pr_L}\right)\left(\frac{u^2}{2}\right)_y\right]_y \tag{B25}$$

APPENDIX C

CALCULATION PROCEDURE

For ease of reference, the transformed momentum and energy equations with their respective boundary conditions are repeated.

Momentum

$$\left(\mathscr{P}_f\right)_\gamma + A_M \mathscr{P}_f = B_M \tag{C1}$$

where

$$A_M = \frac{D_2 f \delta}{\overline{C}_1} \tag{C2}$$

$$B_M = -\delta^3 \beta \left[\frac{1}{(\rho/\rho_e)} - \left(\frac{f_\gamma}{\delta}\right)^2\right] \tag{C3}$$

$$\mathscr{P}_f = \overline{C}_1 f_{\gamma\gamma} \tag{C4}$$

and

$$f = f_\gamma = 0 \quad \text{at} \quad \gamma = 0 \tag{C5}$$

$$\left.\begin{aligned} f_\gamma &= \delta \\ f_{\gamma\gamma} &= 10^{-3}\delta^2 \end{aligned}\right\} \text{ at } \gamma = 1.0 \tag{C6}$$

Energy

$$\left(\mathscr{P}_g\right)_\gamma + A_E \mathscr{P}_g = B_E \tag{C7}$$

where

$$A_E = \frac{D_2 \delta f}{\overline{C}_2} \tag{C8}$$

$$B_E = -\frac{2D_3}{\delta^2}\left\{C\left(1 - \frac{1}{Pr_L}\right)f_\gamma f_{\gamma\gamma}\right\}_\gamma \tag{C9}$$

and

$$\mathscr{P}_g = \overline{C}_2 g_\gamma \tag{C10}$$

$$\left.\begin{aligned} g &= g_w \quad \text{at } \gamma = 0 \\ g &= 1.0 \quad \text{at } \gamma = 1.0 \end{aligned}\right\} \tag{C11}$$

$$g_\gamma = 10^{-3}\delta \quad \text{at } \gamma = 1.0 \tag{C12}$$

It should be noted here that the two equations are overdetermined since conditions (6) and (12) are not needed to solve the set. However, these conditions are satisfied, as it shall be seen, when a numerically correct δ is found.

Solution of the Momentum and Energy Equations

If for a given δ and the coefficients, A_M, B_M, A_E, and B_E are assumed to be functions of γ only. Then the equation set becomes linear and uncoupled. This set is easily solved in the following manner.

Momentum

$$\mathscr{P}_f = \frac{1}{\omega_M}\int_0^\gamma \omega_M B_M d\gamma + \frac{K_1}{\omega_M} \tag{C13}$$

$$f_{\gamma\gamma} = \frac{\mathscr{P}_f}{\overline{C}_1} \tag{C14}$$

$$f_\gamma = \int_0^\gamma f_{\gamma\gamma} d\gamma + K_2 \tag{C15}$$

$$f = \int_0^{\gamma} f_{\gamma} d\gamma + K_3 \tag{C16}$$

where

$$\omega_M = e^{\int_0^{\gamma} A_M d\gamma} \tag{C17}$$

$$K_1 = \frac{\delta - \int_0^1 \frac{1}{\omega_M \overline{\overline{C}}_1} \left(\int_0^1 A_M B_M d\gamma \right) d\gamma}{\int_0^1 \frac{d\gamma}{\omega_M \overline{\overline{C}}_1}} \tag{C18}$$

$$K_2 = K_3 = 0 \tag{C19}$$

Energy

$$\mathscr{P}_g = \frac{1}{\omega_E} \int_0^{\gamma} \omega_E B_E d\gamma + \frac{K_4}{\omega_E} \tag{C20}$$

$$g_{\gamma} = \frac{\mathscr{P}_g}{\overline{\overline{C}}_2} \tag{C21}$$

$$g = \int_0^{\gamma} g_{\gamma} d\gamma + K_5 \tag{C22}$$

where

$$\omega_E = e^{\int_0^{\gamma} A_E d\gamma} \tag{C23}$$

$$K_4 = \frac{1 - g_w - \int_0^1 \frac{1}{\overline{C}_2 \omega_E} \left(\int_0^1 \omega_E B_E d\gamma \right) d\gamma}{\int_0^1 \frac{d\gamma}{\omega_E \overline{C}_2}} \tag{C24}$$

$$K_5 = g_w \tag{C25}$$

Calculational Procedure at a Given Axial Position (Stepping-Up-Process)

First define a montonic increasing sequence of δ's as $\delta_{i+1} = \delta_i + \Delta\delta$. For this report, it was found that

$$\Delta\delta \approx \frac{1}{1 + M_e}$$

gives a good variation through the entire nozzle. Next, let the notation $f_{i,k}$ and $g_{i,k}$ mean f and g as a function of and an iteration index K. Figure 19 shows the general flow diagram outlining the stepping-up-process calculation method and is further described by the following detailed steps:

Step (1): From the tabulated input of X, r, T_W, and Pe/Po, compute all free-stream conditions, such as D_2, T_e, M_e, ρ_w, ρ_e, μ_w, β, D_1, R, g_w, and D_3.

Step (2): Setting i = k = 1, that is, for an initial δ and a first iteration, estimate starting values of $f_{i,\kappa}$, $(f_{i,\kappa})_\gamma$, $(f_{i,\kappa})_{\gamma\gamma}$, $g_{i,\kappa}$, and $(g_{i,\kappa})_\gamma$ by the 1/7 power law or from values of previous axial positions.

Step (3): Compute the coefficients A_M, B_M, A_E, and B_E. In the evaluation of $\overline{C}_1$ and $\overline{C}_2$, it is necessary to find a continuous $\epsilon_{m,i}$ (eddy diffusivity coefficient), derived from the combination of $\epsilon_{m,1}$, $\epsilon_{m,2}$, and $\epsilon_{m,3}$. This is done by defining γ_2 as the point where $y_1^+(\gamma) = 12$, and γ_3 as the position where $\epsilon_{m,2} = \epsilon_{m,3}$. During the iterative process it was found advisable to not let γ_2 or γ_3 vary more than 40 percent from the previous iteration. This proved to have a stabilizing effect on the solutions, and in the case of high β's, a faster convergence rate.

Step (4): Using equations (C13) to (C19) solve for $f_{i,\kappa+1}$, $(f_{i,\kappa+1})_\gamma$ and $(f_{i,\kappa+1})_{\gamma\gamma}$. It was advisable to underrelax the functions for damping oscillatory behavior.

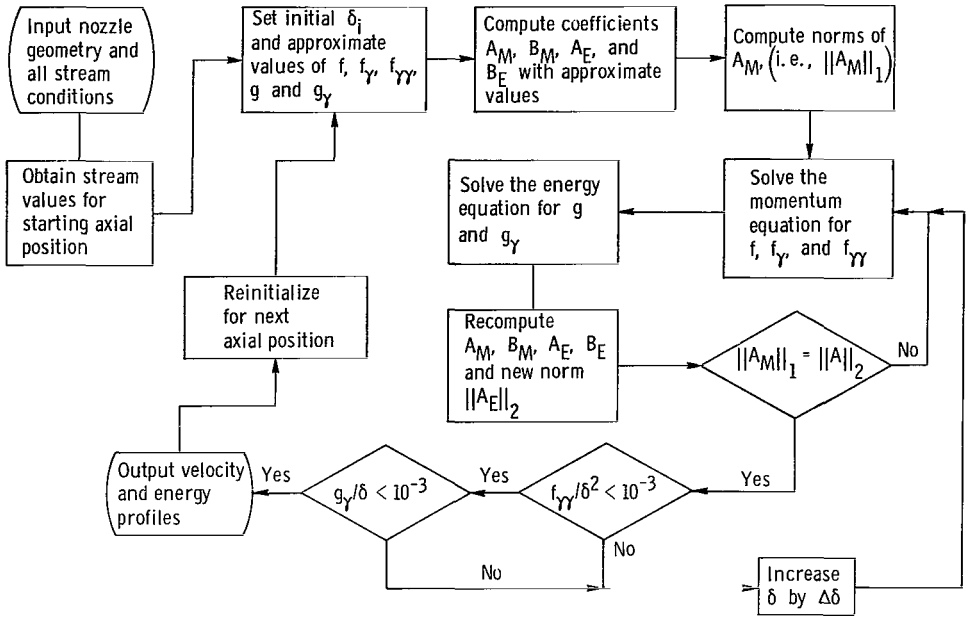

Figure 19. - General flow diagram for the boundary layer calculation.

Step (5): Solve equations (C20) to (C25) for $g_{i,K+1}$ and $(g_{i,K+1})_\gamma$. Again underrelaxation was used. In both steps (4) and (5), all integrations were done with a modified Simpson's rule routine. For the term B_E a central differencing scheme was used.

Step (6): Recalculate the coefficients A_M, B_M, A_E, and B_E using the values of the $K + 1^{th}$ iteration step. If there is no significant change in these functions, proceed to step (7), otherwise return to step (4).

Step (7): Now evaluate $f_{\gamma\gamma}/\delta^2$ and g_γ/δ at the edge and check if these values are within the specified limits, (i.e., 10^{-3}). If the tolerance criteria is met, all conditions are satisfied and the solution is completed at this axial position. However, if the criteria is not met, one must increase δ by $\Delta\delta$, set $K = 1$ and return to step (2) using the last values of f, f_γ, $f_{\gamma\gamma}$, g and g_γ as initial estimates.

REFERENCES

1. Bartz, D. R.: Turbulent Boundary-Layer Heat Transfer from Rapidly Accelerating Flow of Rocket Combustion Gases and of Heated Air. Advances in Heat Transfer. Vol. 2. James P. Hartnett and Thomas F. Irvine, Jr., eds., Academic Press, 1965, pp. 1-108.

2. Smith, A. M. O.; and Cebeci, T.: Numerical Solution of the Turbulent-Boundary-Layer Equations. Rep. DAC-33735, Douglas Aircraft Co., Inc., May 29, 1967. (Available from DDC as AD-656430.)

3. Herring, H. James; and Mellor, George L.: A Method of Calculating Compressible Turbulent Boundary Layers. NASA CR-1144, 1968.

4. Patanker, S. V.; and Spalding, D. B.: Heat and Mass Transfer in Boundary Layers. International Textbook, 1968.

5. Bushnell, Dennis M.; and Beckwith, Ivan E.: Calculation of Nonequilibrium Hypersonic Turbulent Boundary Layers and Comparisons with Experimental Data. AIAA J., vol. 8, no. 8, Aug. 1970, pp. 1462-1469.

6. Boldman, Donald R.; Schmidt, James F.; and Fortini, Anthony: Turbulence, Heat-Transfer, and Boundary Layer Measurements in a Conical Nozzle with a Controlled Inlet Velocity Profile. NASA TN D-3221, 1966.

7. Boldman, Donald R.; Neumann, Harvey E.; and Schmidt, James F.: Heat Transfer in 30° and 60° Half-Angle of Convergence Nozzles with Various Diameter Uncooled Pipe Inlets. NASA TN D-4177, 1967.

8. Boldman, Donald R.; Schmidt, James F.; and Ehlers, Robert C.: Experimental and Theoretical Turbulent Boundary Layer Development in a Mach 4.4 Water-Cooled Conical Nozzle. NASA TN D-5377, 1969.

9. Deissler, R. G.; and Loeffler, A. L., Jr.: Analysis of Turbulent Flow and Heat Transfer on a Flat Plate at High Mach Numbers with Variable Fluid Properties. NASA TR R-17, 1959.

10. Van Driest, E. R.: On Turbulent Flow Near a Wall. J. Aeron. Soc., vol. 23, no. 11, Nov. 1956, pp. 1007-1011, 1036.

11. Clauser, F. H.: The Turbulent Boundary Layer. Advances in Applied Mechanics. Vol. IV. Richard von Mises and Theodore von Karman, eds., Academic Press, 1956.

12. Schmidt, James F.: Effects of a Magnetic Field on the Conduction Heat Transfer at the Stagnation Point of a Partially-Ionized Argon Gas. NASA TN D-3251, 1966.

13. Cohen, Clarence B.; and Reshotko, Eli: The Compressible Laminar Boundary Layer with Heat Transfer and Arbitrary Pressure Gradient. NACA Rep. 1294, 1956.

14. Cohen, Nathaniel B.: Boundary-Layer Similar Solutions and Correlation Equations for Laminar Heat-Transfer Distribution in Equilibrium Air at Velocities up to 41,000 feet per second. NASA TR R-118, 1961.

15. Back, L. H.; Massier, P. F.; and Cuffel, R. F.: Flow Phenomena and Convective Heat Transfer in a Conical Supersonic Nozzle. J. Spacecraft Rockets, vol. 4, no. 8, Aug. 1967, pp. 1040-1047.

16. Schlichting, Hermann (J. Kestin, trans.): Boundary Layer Theory. Second ed., McGraw-Hill Book Co., Inc., 1955.

TABLE I. - NOZZLE CONFIGURATION

Station	Axial distance, z		Diameter-D		Uncooled inlet			Cooled inlet		
	cm	in.	cm.	in.	Turbulent boundary-layer distance, x		Ratio of nozzle to throat distance, x/x_T	Turbulent boundary-layer distance, x		Ratio of nozzle to throat distance, x/x_T
					cm	in.		cm	in.	
2	-11.468	-4.515	15.875	6.25	41.30	16.255	0.7602	93.57	36.84	0.8776
3	-8.928	-3.515	12.934	5.092	44.22	17.41	.8139	96.52	38.00	.9052
[a]4	-6.380	-2.512	9.992	3.934	47.17	18.57	.8682	99.47	39.16	.9328
5	-5.481	-2.158	8.961	3.528	48.21	18.98	.8873	100.5	39.57	.9426
6	-4.602	-1.812	7.945	3.128	49.23	19.38	.9060	101.5	39.97	.9521
7	-3.708	-1.460	6.914	2.722	50.24	19.78	.9247	102.5	40.37	.9616
8	-2.819	-1.110	5.883	2.316	51.28	20.19	.9439	103.6	40.78	.9714
9	-1.557	-.613	4.470	1.760	52.71	20.75	.9701	105.0	41.34	.9847
10	-.445	-.175	3.835	1.510	53.87	21.21	.9916	106.2	41.80	.9957
11	0	0	3.790	1.492	54.33	21.39	1.000	106.6	41.98	1.000
12	.330	.130	3.815	1.502	54.66	21.52	1.006	107.0	42.11	1.003
13	.648	.255	3.912	1.540	54.97	21.64	1.012	107.3	42.23	1.006
14	.996	.392	4.074	1.604	55.32	21.78	1.018	107.6	42.37	1.009
15	1.615	.634	4.399	1.732	55.98	22.04	1.030	108.3	42.63	1.015
[a]16	3.101	1.221	5.187	2.042	57.51	22.64	1.058	109.8	43.23	1.030
17	6.949	2.736	7.259	2.858	61.49	24.21	1.132	113.8	44.80	1.067
[a]18	13.889	5.468	10.978	4.322	68.68	27.04	1.264	121.0	47.63	1.135
19	20.831	8.201	14.712	5.792	75.87	29.87	1.396	128.2	50.46	1.202
[a]19a	24.181	9.520	16.520	6.504	79.86	31.44	1.470	131.7	51.84	1.234
20	28.021	11.032	18.543	7.320	83.31	32.80	1.533	135.6	53.39	1.272

[a]Boundary layer probing stations.

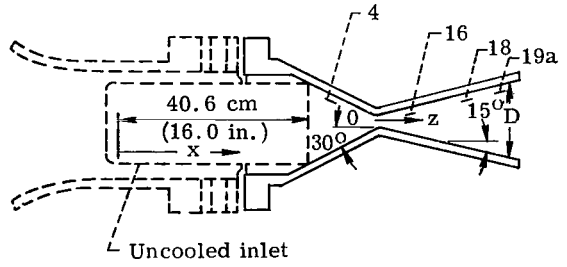

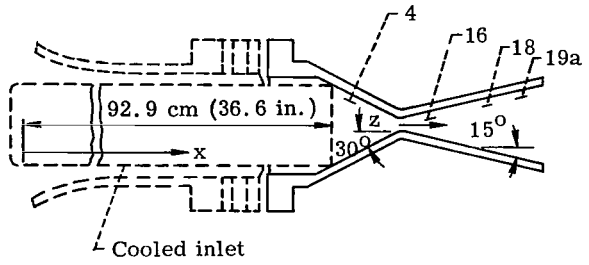

TABLE II. - NOZZLE FLOW PARAMETERS

Station	Mach number, M_e	Ratio of kinetic to total energy, D_6	Pressure ratio, P_e/P_0	Uncooled inlet with boundary-layer bled off nozzle entrance			Uncooled inlet			Cooled Inlet		
				Ratio of nozzle to throat distance, x/x_T	Velocity gradient parameter, β	Nozzle geometry parameter, R	Ratio of nozzle to throat distance, x/x_T	Velocity gradient parameter, β	Nozzle geometry parameter, R	Ratio of nozzle to throat distance, x/x_T	Velocity gradient parameter, β	Nozzle geometry parameter, R
2	0.02778	0.00022	0.99946	0.0480	0.06224	-0.0840	0.7602	3.555	-5.366	0.8776	8.0418	-12.162
3	.04678	.00043	.99846	.2622	1.048	-.5534	.8139	12.91	-6.834	.9052	28.168	-14.918
[a]4	.07894	.00123	.99565	.4770	2.723	-1.315	.8682	19.67	-9.508	.9328	41.476	-20.056
5	.09841	.001925	.99325	.5527	3.5782	-1.700	.8873	22.79	-10.84	.9426	47.514	-22.599
6	.1266	.003193	.98887	.6268	4.4261	-2.156	.9060	25.38	-12.37	.9521	52.409	-25.523
7	.1684	.00517	.9804	.7021	5.883	-2.808	.9247	30.74	-14.69	.9616	62.733	-29.983
8	.2350	.01118	.9624	.7774	10.22	-3.845	.9439	49.20	-18.54	.9714	99.383	-37.443
9	.5050	.05152	.8399	.8825	12.79	-3.438	.9701	55.75	-15.01	.9847	111.24	-29.903
10	.9281	.1466	.5733	.9675	10.10	-2.065	.9916	41.07	-8.405	.9957	81.549	-17.078
11	1.114	.1984	.4600	1.0000	8.826	≈0.0	1.000	35.01	≈0.00	1.000	68.741	≈0.0
12	1.275	.2602	.3733	1.0241	7.246	0.8549	1.006	28.24	3.350	1.003	55.212	6.5465
13	1.485	.3124	.2785	1.0476	5.996	2.121	1.012	22.98	8.133	1.006	44.761	15.877
14	1.681	.3472	.2084	1.0737	4.455	2.948	1.018	16.77	11.10	1.009	32.511	21.611
15	1.771	.3852	.1824	1.1201	2.317	3.565	1.030	8.45	13.02	1.015	16.339	25.17
[a]16	2.082	.4634	.1125	1.2328	1.639	3.323	1.058	5.58	11.33	1.030	10.66	21.627
17	2.789	.6069	.0375	1.5236	.913	2.986	1.132	2.69	8.806	1.067	4.977	16.294
[a]18	3.739	.7362	.0094	2.0485	.4607	2.645	1.264	1.131	6.482	1.135	1.987	11.416
19	4.416	.7957	.0038	2.5734	.262	2.493	1.396	.563	5.370	1.202	.951	9.0655
[a]19a	4.640	.8121	------	------	.167	2.445	1.470	.310	4.974	1.234	.513	8.222
20	4.784	.8205	.0024	3.1167	.0532	2.407	1.533	.104	4.701	1.272	.118	7.641

[a]Boundary-layer probing stations.

TABLE III. - TYPICAL SOLUTIONS FOR UNCOOLED INLET WITH BOUNDARY LAYER

BLED OFF AT NOZZLE ENTRANCE

(a) Station 9; ratio of nozzle to throat distance, 0.8825; velocity gradient parameter, 12.79; turbulent Prandtl number, 1.9877

Transformed boundary layer coordinate, η	Velocity ratio, f_η	Derivative of velocity ratio, $f_{\eta\eta}$	Shear-stress function, $\mathscr{P}_f$	Total enthalpy, ratio, g	Derivative of total enthalpy g_η	Heat-transfer function, $\mathscr{P}_g$	Coordinate normal to nozzle surface, y	
							cm	in.
0	0	12.548	8.8308	0.8710	0.4763	0.5828	0	0
.002465	.03107	12.448	8.8097	.8722	.4870	.5968	.00001196	.000004708
.004930	.06148	12.244	8.7886	.8734	.4954	.6102	.00002393	.000009421
.007396	.09145	11.913	8.7675	.8746	.5010	.6224	.00003592	.00001414
.01479	.1750	10.552	8.7048	.8783	.5009	.6499	.00007196	.00002833
.02465	.2690	8.4965	8.6231	.8831	.4707	.6659	.0001201	.00004730
.03451	.3441	6.7725	8.5444	.8876	.4260	.6675	.0001685	.00006632
.04437	.4044	5.4741	8.4689	.8915	.3805	.6631	.0002169	.00008539
.06409	.4944	3.7958	8.3279	.8982	.3039	.6504	.0003139	.0001236
.08628	.5659	2.7281	8.1839	.9043	.2420	.6377	.0004234	.0001667
.1159	.6129	2.0901	8.0107	.9089	.05204	.6274	.0005697	.0002243
.1824	.6637	.9095	7.6695	.9120	.04650	.6020	.0008992	.0003540
.2194	.6851	.4926	7.4935	.9139	.05686	.5916	.001083	.0004261
.3210	.7150	.3586	7.2108	.9172	.04782	.5878	.001395	.0005492
.5517	.7735	.1889	6.3143	.9255	.02829	.5760	.002543	.001001
.8978	.8220	.1115	5.2265	.9338	.02089	.5589	.004270	.001681
1.1286	.8468	.09943	4.6078	.9395	.02624	.5425	.005425	.002136
1.4747	.8782	.08060	3.7972	.9484	.02486	.5088	.007167	.002822
1.8208	.9038	.06501	3.1149	.9567	.02306	.4672	.008928	.003515
2.0515	.9180	.05619	2.7235	.9618	.02167	.4361	.01010	.003978
2.6284	.9455	.03876	1.9347	.9732	.01772	.3511	.01307	.005144
3.3206	.9671	.02465	1.2737	.9838	.01271	.2479	.01665	.006557
4.0128	.9806	.01566	.8368	.9910	.008229	.1585	.02027	.007981
4.9358	.9906	.008647	.4814	.9964	.003912	.07454	.02512	.009890
6.0895	.9964	.004205	.2466	.9991	.001187	.02247	.03122	.01229
6.7817	.9981	.002739	.1668	.9997	.0005051	.009541	.03487	.01373
7.3586	.9990	.001907	.1206	.9999	.0002288	.004318	.03790	.01492
8.0508	.9996	.001219	.08157	1.0000	.00008027	.001514	.04155	.01636
8.9738	1.0000	.0006808	.04768	1.0000	.00001674	.0003157	.04643	.01828

TABLE III. - Continued. TYPICAL SOLUTIONS FOR UNCOOLED INLET WITH BOUNDARY LAYER BLED OFF AT NOZZLE ENTRANCE

(b) Station 11 (throat); ratio of nozzle to throat distance, 1.0000; velocity gradient parameter, 8.826; turbulent Prandtl number, 2.1494

Transformed boundary layer coordinate, η	Velocity ratio, f_η	Derivative of velocity ratio, $f_{\eta\eta}$	Shear-stress function, $\mathscr{P}_f$	Total enthalpy ratio, g	Derivative of total enthalpy ratio, g_η	Heat-transfer function, $\mathscr{P}_g$	Coordinate normal to nozzle surface, y	
							cm	in.
0	0	17.831	8.6913	0.8569	0.7723	0.5302	0	0
.001950	.03484	17.682	8.6729	.8585	.8410	.5783	.00001300	.000005118
.003900	.06917	17.302	8.6545	.8602	.9014	.6238	.00002545	.00001002
.005850	.1025	16.727	8.6362	.8620	.9502	.6645	.00003820	.00001504
.01170	.1942	14.337	8.5817	.8678	1.0154	.7489	.00007648	.00003011
.01755	.2710	11.809	8.5285	.8737	0.9836	.7822	.0001147	.00004517
.02535	.3523	9.0688	8.4603	.8809	.8752	.7823	.0001656	.00006521
.03510	.4288	6.7218	8.3796	.8887	.7284	.7579	.0002290	.00009014
.05655	.5402	3.9939	8.2186	.9016	.4934	.7004	.0003673	.0001446
.07995	.6030	1.2720	8.0646	.9096	.1727	.5893	.0005166	.0002034
.1268	.6501	0.7974	7.7896	.9161	.1134	.5681	.0008138	.0003204
.1736	.6818	.5750	7.5365	.9207	.08478	.5564	.001109	.0004368
.2539	.7070	.4396	7.2847	.9244	.06716	.5491	.001423	.0005604
.4364	.7645	.2279	6.4762	.9336	.03871	.5299	.002563	.001009
.7102	.8115	.1498	5.4724	.9420	.02812	.5110	.004257	.001676
.9840	.8458	.1121	4.6194	.9491	.02494	.4899	.005944	.002340
1.1665	.8653	.09946	4.1154	.9536	.02398	.4730	.007061	.002780
1.4403	.8905	.08291	3.4474	.9599	.02236	.4431	.008735	.003439
1.7141	.9114	.06891	2.8754	.9658	.02057	.4089	.01041	.004097
2.2617	.9430	.04719	1.8763	.9760	.01665	.3322	.01374	.005408
2.7180	.9613	.03413	1.4300	.9829	.01332	.2659	.01651	.006500
3.1743	.9742	.02449	1.0257	.9882	.01018	.2033	.01929	.007594
3.8131	.9859	.01521	.6361	.9935	.006466	.1289	.02318	.009125
4.1782	.9903	.01152	.4815	.9955	.004782	.09525	.02540	.01000
4.6345	.9940	.008108	.3384	.9973	.003139	.06247	.02817	.01109
5.5471	.9979	.003960	.1652	.9992	.001168	.02321	.03373	.01328
6.1859	.9990	.002354	.09160	.9997	.0005193	.01032	.03764	.01482
7.1898	.9998	.0009875	.04116	1.0000	.0001188	.002360	.04376	.01723
7.7374	1.0000	.0006062	.02527	1.0000	.00004774	.0009483	.04709	.01854

TABLE III. - Concluded. TYPICAL SOLUTIONS FOR UNCOOLED INLET WITH BOUNDARY LAYER BLED OFF AT NOZZLE ENTRANCE

(c) Station 20; ratio of nozzle to throat distance, 3.1167; velocity gradient parameter, 0.0532; turbulent Prandtl number, 1.8532

Transformed boundary layer coordinate, η	Velocity ratio, f_η	Derivative of velocity ratio, $f_{\eta\eta}$	Shear-stress function $\mathscr{P}_f$	Total enthalpy ratio, g	Derivative of total enthalpy ratio, g_η	Heat-transfer function, $\mathscr{P}_g$	Coordinate normal to nozzle surface, y	
							cm	in.
0	0	84.417	0.2483	0.5866	16.832	0.05229	0	0
.0005187	.04377	84.192	.2482	.5959	18.556	.05613	.0005441	.0002142
.001037	.08712	82.753	.2481	.6058	19.994	.05987	.001094	.0004307
.001556	.1294	80.289	.2480	.6166	21.178	.06340	.001648	.0006488
.002593	.2092	73.156	.2477	.6394	22.475	.06952	.002761	.001087
.004149	.3131	60.251	.2473	.6743	22.099	.07581	.004417	.001739
.005705	.3972	48.159	.2468	.7072	19.950	.07882	.006035	.002376
.007261	.4642	38.322	.2462	.7361	17.277	.07942	.007607	.002995
.009336	.5330	28.668	.2453	.7684	13.902	.07810	.009622	.003788
.01504	.6507	14.790	.2428	.8283	7.8290	.07131	.01475	.005809
.02126	.7094	4.4825	.2405	.8564	5.1057	.06521	.01983	.007807
.03060	.7438	3.0663	.2379	.8732	3.2285	.05522	.02697	.01062
.03994	.7686	2.3131	.2353	.8870	1.8321	.05371	.03378	.01330
.05083	.7907	1.7746	.2323	.8995	1.0541	.05238	.04143	.01631
.09180	.8349	1.0139	.2230	.9276	.5143	.04937	.06314	.02486
.1403	.8720	0.5830	.2101	.9463	.2899	.04576	.09230	.03634
.1889	.8952	.3944	.1980	.9577	.1916	.04261	.1191	.04688
.2617	.9182	.2548	.1812	.9687	.1192	.03833	.1563	.06154
.3345	.9337	.1821	.1657	.9761	.1121	.03447	.1910	.07519
.4559	.9517	.1187	.1422	.9864	.06223	.02854	.2452	.09654
.5773	.9638	.08354	.1211	.9922	.03905	.02173	.2951	.1166
.7229	.9740	.05846	.09863	.9967	.02024	.01529	.3541	.1394
.8928	.9822	.04015	.07601	.9989	.007382	.008904	.4181	.1646
1.0142	.9865	.03126	.06202	.9995	.003431	.005651	.4623	.1820
1.1355	.9899	.02456	.04971	.9998	.001520	.003470	.5050	.1988
1.2812	.9930	.01841	.03699	1.0000	.0004267	.001834	.5550	.2185
1.6453	.9979	.009569	.01332	1.0000	.00002098	.0002395	.6756	.2660
1.7666	.9989	.007178	.007494	1.0000	.00002098	.0001058	.7150	.2815
2.0579	1.0000	.001080	.0009765	1.0000	.00002098	.0001018	.8080	.3181

TABLE IV. - TYPICAL SOLUTIONS FOR UNCOOLED INLET

(a) Station 9; ratio of nozzle to throat-distance, 0.9701; velocity gradient parameter, 55.75; turbulent Prandtl number, 3.7232

Transformed boundary layer coordinate, η	Velocity ratio, f_η	Derivative of velocity ratio, $f_{\eta\eta}$	Shear-stress function, $\mathscr{P}_f$	Total enthalpy ratio, g	Derivative of total enthalpy ratio, g_η	Heat-transfer function, $\mathscr{P}_g$	Coordinate normal to nozzle surface, y	
							cm	in.
0	0	33.125	28.773	0.8710	0.8116	0.6827	0	0
.001314	.04358	32.791	28.705	.8721	.8551	.7086	.00001332	.000005243
.002629	.08636	31.956	28.638	.8732	.8920	.7337	.00002664	.00001049
.003943	.1278	30.714	28.572	.8744	.9208	.7571	.00003998	.0001574
.007887	.2400	25.756	28.376	.8782	.9840	.8136	.00008006	.00003152
.01314	.3583	19.377	28.130	.8827	.6690	.8535	.0001336	.00005260
.01972	.4122	5.9234	27.846	.8862	.4779	.7540	.0002006	.00007896
.02629	.4463	4.5395	27.573	.8891	.4045	.7466	.0002674	.0001054
.06178	.5505	1.9743	26.229	.8988	.2458	.7178	.0006312	.0002485
.08544	.5900	1.4200	25.421	.9031	.1956	.7092	.0008745	.0003443
.1170	.6282	1.0248	24.419	.9080	.1454	.7017	.001199	.0004722
.1711	.6585	.7855	23.422	.9139	.1083	.6967	.001547	.0006092
.2942	.7275	.4045	20.238	.9239	.06599	.6822	.002827	.001113
.4172	.7682	.2864	17.544	.9313	.05640	.6707	.004112	.001619
.5402	.8015	.2500	15.167	.9381	.05383	.6598	.005405	.002128
.6633	.8306	.2175	13.068	.9446	.05198	.6475	.006701	.002638
.8478	.8672	.1753	10.391	.9539	.04839	.6245	.008656	.003408
1.0324	.8967	.1404	8.2103	.9624	.04390	.5960	.01063	.004183
1.2169	.9202	.1116	6.4510	.9700	.03876	.5622	.01263	.004963
1.4630	.9440	.08146	4.6439	.9787	.03139	.5105	.01527	.006011
1.7091	.9612	.05893	3.3233	.9855	.02410	.4530	.01794	.007063
1.9551	.9734	.04239	2.3713	.9906	.01752	.3934	.02063	.008122
2.2627	.9836	.02803	1.5578	.9949	.01087	.3187	.02400	.009450
2.5703	.9900	.01868	1.0340	.9975	.006184	.2482	.02738	.01078
2.9394	.9946	.01176	.6498	.9991	.002801	.1747	.03145	.01238
3.5546	.9979	.005824	.3214	1.0000	.0005839	.08567	.03823	.01505
4.0467	.9990	.003197	.1765	1.0000	.0004584	.04315	.04364	.01718
4.4158	.9995	.001984	.1095	1.0000	.0004584	.02411	.04773	.01879
5.154	1.0000	.0007336	.04051	1.0000	.0004584	.006325	.05580	.02200

TABLE IV. - Continued. TYPICAL SOLUTIONS FOR UNCOOLED INLET

(b) Station 11 (throat); ratio of nozzle to throat distance, 1.000; velocity gradient parameter, 35.01; turbulent Prandtl number, 3.9191

Transformed boundary layer coordinate η	Velocity ratio, f_η	Derivative of velocity ratio, $f_{\eta\eta}$	Shear-stress function, $\mathscr{P}_f$	Total enthalpy ratio, g	Derivative of total enthalpy ratio, g_η	Heat-transfer function, $\mathscr{P}_g$	Coordinate normal to nozzle surface, y	
							cm	in.
0	0	45.335	22.098	0.8569	1.2524	0.5883	0	0
.001123	.05081	44.746	22.056	.8585	1.5170	.6744	.00001458	.000005742
.002246	.1004	43.195	22.014	.8603	1.7476	.7568	.00002918	.00001149
.003368	.1479	40.924	21.972	.8624	1.9748	.8322	.00004376	.00001723
.005614	.2339	35.50	21.890	.8672	2.1634	.9543	.00007295	.00002872
.008982	.3393	27.267	21.773	.8735	1.5251	1.0614	.0001165	.00004586
.01010	.3620	10.762	21.736	.8750	1.2612	1.0799	.0001309	.00005155
.01347	.3925	8.3346	21.627	.8785	.9105	.8783	.0001742	.00006860
.02246	.4511	5.1688	21.348	.8853	.6435	.7503	.0002893	.0001139
.03593	.5062	3.2668	20.952	.8924	.4571	.7060	.0004615	.0001817
.05614	.5587	2.0816	20.404	.8986	.3515	.6722	.0008965	.0002828
.08645	.6090	1.3330	19.644	.9061	.2392	.6462	.001375	.0004337
.1462	.6546	.8779	18.675	.9158	.1463	.6282	.002038	.0006430
.1987	.6928	.6038	17.574	.9222	.1072	.6129	.002861	.0009026
.3038	.7417	.3598	15.620	.9313	.07353	.5935	.004501	.001420
.4615	.7900	.2785	13.087	.9420	.06430	.5725	.006942	.002190
.5665	.8177	.2459	11.591	.9486	.06104	.5599	.008565	.002702
.7767	.8637	.1906	9.0208	.9606	.05338	.5291	.01180	.003722
.9869	.8993	.1464	6.9476	.9709	.04468	.4898	.01503	.004740
1.1971	.9264	.1114	5.2969	.9794	.03571	.4441	.01824	.005755
1.4073	.9468	.08392	3.9987	.9860	.02719	.3939	.02145	.006768
1.5649	.9587	.06744	3.2184	.9898	.02145	.3548	.02386	.007528
1.9327	.9777	.03972	1.9035	.9956	.01102	.2644	.02947	.009298
2.1429	.9846	.02906	1.3961	.9975	.007007	.2165	.03268	.01031
2.4056	.9904	.01952	.9407	.9989	.003694	.1630	.03668	.01157
3.0361	.9972	.007445	.3607	1.0000	.0005550	.07073	.04625	.01459
3.5090	.9990	.003660	.1777	1.0000	.0004773	.03269	.05341	.01685
3.8243	.9995	.002307	.1121	1.0000	.0004773	.01820	.05820	.01836
4.4623	1.0000	.0009944	.04834	1.0000	.0004773	.005355	.06695	.02112

TABLE IV. - Concluded. TYPICAL SOLUTIONS FOR UNCOOLED INLET

(c) Station 20; ratio of nozzle to throat distance, 1.533; velocity gradient parameter, 2.3985; turbulent Prandtl number, 2.3985

Transformed boundary layer coordinate, η	Velocity ratio, f_η	Derivative of velocity ratio, $f_{\eta\eta}$	Shear-stress function, $\mathscr{P}_f$	Total enthalpy ratio, g	Derivative of total enthalpy ratio, g_η	Heat-transfer function, $\mathscr{P}_g$	Coordinate normal to nozzle surface, y	
							cm	in.
0	0	126.13	0.3708	0.5866	22.703	0.06508	0	0
.0002803	.03545	125.94	.3707	.5933	24.984	.06941	.0004110	.0001618
.0005619	.07067	124.50	.3706	.6006	27.011	.07367	.0008255	.0003250
.0008428	.1053	121.95	.3705	.6085	28.823	.07779	.001242	.0004891
.001686	.2032	109.36	.3702	.6345	32.235	.08872	.002496	.0009827
.002248	.2618	98.766	.3699	.6526	32.170	.09443	.003335	.001313
.003090	.3383	82.851	.3694	.6810	31.096	.1004	.004572	.001800
.004776	.4186	24.478	.3685	.7115	12.469	.1047	.006975	.002746
.008147	.4822	14.771	.3668	.7452	8.0796	.07779	.01166	.004592
.01320	.5401	8.9943	.3641	.7729	5.8743	.07382	.01849	.007278
.01910	.5836	6.1173	.3608	.7970	4.2045	.07114	.02616	.01030
.02332	.6068	4.9643	.3584	.8114	3.2849	.06977	.03155	.01242
.02669	.6224	4.2918	.3565	.8205	2.8083	.06886	.03579	.01409
.06288	.7101	1.8287	.3380	.8791	1.1460	.06332	.07407	.02916
.1023	.7754	1.4772	.3119	.9169	.8091	.05836	.1176	.04630
.1418	.8269	1.1423	.2819	.9438	.5672	.05294	.1570	.06182
.1681	.8543	.9504	.2612	.9570	.4391	.04890	.1812	.07133
.2207	.8960	.6522	.2215	.9749	.2570	.04062	.2251	.08861
.2732	.9246	.4509	.1859	.9853	.1490	.03282	.2642	.1040
.3127	.9402	.3460	.1624	.9902	.09927	.02762	.2911	.1146
.3784	.9587	.2284	.1290	.9949	.05105	.02036	.3322	.1308
.4573	.9731	.1445	.09718	.9977	.02340	.01385	.3769	.1484
.5362	.9824	.09443	.07248	.9990	.01083	.009271	.4191	.1650
.6414	.9900	.05529	.04806	.9997	.003824	.005316	.4714	.1856
.7466	.9945	.03281	.03094	1.0000	.001281	.002969	.5215	.2053
.8912	.9979	.01582	.01591	1.0000	.0008748	.001264	.5880	.2315
.9813	.9990	.009714	.009994	1.0000	.0008748	.0007049	.6294	.2478
1.0358	.9995	.007269	.007546	1.0000	.0008748	.000496	.6533	.2572
1.1279	1.0000	.004281	.004492	1.0000	.0008748	.0002582	.6944	.2734

TABLE V. - TYPICAL SOLUTIONS FOR COOLED INLET

(a) Station 9; ratio of nozzle to throat distance, 0.9847; velocity gradient parameter, 111.24; turbulent Prandtl number, 5.1688

Transformed boundary layer coordinate, η	Velocity ratio, f_η	Derivative of velocity ratio, $f_{\eta\eta}$	Shear-stress function, $\mathscr{P}_f$	Total enthalpy ratio, g	Derivative of total enthalpy ratio, g_η	Heat-transfer function, $\mathscr{P}_g$	Coordinate normal to nozzle surface, y	
							cm	in.
0	0	45.842	40.232	0.8473	1.1873	0.9172	0	0
.0009864	.04524	45.339	40.134	.8485	1.2551	.9497	.00001372	.00000540
.001973	.08961	44.072	40.032	.8497	1.3102	.9811	.00002746	.00001081
.002959	.1324	42.199	39.94	.8511	1.3471	1.0107	.00004120	.00001622
.004932	.2115	37.424	39.749	.8538	1.4402	1.0618	.00006726	.00002707
.007891	.3116	30.031	39.474	.8580	1.3119	1.1150	.0001101	.00004336
.01184	.4091	9.5202	39.135	.8620	.8570	1.1471	.0001654	.00006510
.01775	.4548	6.5823	38.663	.8666	.7083	1.0077	.0002483	.00009774
.02565	.4984	4.6478	38.067	.8716	.5779	.9892	.0003594	.0001415
.04636	.5699	2.5937	36.630	.8799	.4306	.9640	.0006520	.0002567
.06411	.6090	1.8672	35.508	.8855	.3506	.9525	.0009040	.0003559
.08187	.6383	1.4514	34.460	.8905	.2861	.9445	.001157	.0004554
.1284	.6767	1.0383	32.752	.9008	.1959	.9352	.001578	.0006213
.2208	.7453	.5367	28.405	.9148	.1209	.9141	.002939	.001157
.3592	.8002	.2903	23.152	.9289	.09591	.8876	.004966	.001955
.5439	.8513	.2461	17.492	.9454	.08279	.8506	.007699	.003031
.6362	.8730	.2154	15.118	.9528	.07760	.8280	.009078	.003574
.7747	.9006	.1750	12.070	.9630	.06851	.7878	.01116	.004394
.9594	.9293	.1307	8.8407	.9744	.05492	.7251	.01396	.005498
1.1440	.9505	.09614	6.407	.9832	.04119	.6529	.01679	.006612
1.3748	.9689	.06446	4.2425	.9909	.02610	.5543	.02036	.008014
1.6056	.9809	.04293	2.8053	.9956	.01482	.4530	.02313	.009422
1.8826	.9895	.02671	1.7387	.9984	.006496	.3375	.02846	.01140
2.2057	.9949	.01622	1.0548	.9997	.002031	.2224	.03325	.01309
2.4366	.9966	.01170	.7606	1.0000	.00070	.1571	.03686	.01451
2.7135	.9979	.007761	.5048	1.0000	.0006534	.1571	.04117	.01621
3.0828	.9990	.004371	.2844	1.0000	.0006534	.1571	.04691	.01847
3.3598	.9995	.002775	.1805	1.0000	.0006534	.1571	.05123	.02017
3.8676	1.0000	.001160	.07551	1.0000	.0006534	.1571	.05913	.02328

TABLE V. - Continued. TYPICAL SOLUTIONS FOR COOLED INLET

(b) Station 11 (throat); ratio of nozzle to throat distance, 1.000; velocity gradient parameter, 68.741; turbulent Prandtl number, 5.3998

Transformed boundary layer coordinate, η	Velocity ratio, f_η	Derivative of velocity ratio, $f_{\eta\eta}$	Shear-stress function, $\mathscr{P}_f$	Total enthalpy ratio, g	Derivative of total enthalpy ratio, g_η	Heat-transfer function, $\mathscr{P}_g$	Coordinate normal to nozzle surface, y	
							cm	in.
0	0	64.051	31.320	0.8481	1.5825	0.6539	0	0
.0008864	.05669	63.031	31.256	.8497	2.0216	.7589	.00001597	.000006286
.001773	.1117	60.361	31.192	.8517	2.3814	.8594	.00003195	.00001258
.002659	.1639	56.543	31.128	.8541	2.7273	.9519	.00004790	.00001886
.006205	.3337	39.142	30.885	.8635	2.0934	1.2056	.0001116	.00004392
.007091	.3594	15.296	30.827	.8651	1.7728	1.2397	.0001274	.00005015
.01064	.4030	10.641	30.606	.8702	1.2613	1.0109	.0001905	.00007499
.01507	.4430	7.6787	30.340	.8752	1.0197	.8786	.0002692	.0001060
.02571	.5057	4.5690	29.736	.8840	.7153	.8127	.0004577	.0001802
.04698	.5767	2.4822	28.633	.8938	.5061	.7550	.0008234	.0003277
.06559	.6157	1.7574	27.749	.9007	.3792	.7299	.001159	.0004564
.1569	.7040	.7621	24.542	.9214	.1625	.6849	.002515	.0009902
.2813	.7700	.4081	20.336	.9371	.1078	.6494	.004681	.001843
.3643	.8022	.3594	17.901	.9457	.1002	.6311	.006124	.002411
.4473	.8304	.3153	15.701	.9537	.09293	.6145	.007564	.002978
.5717	.8663	.2574	12.812	.9645	.08045	.5857	.009721	.003827
.6962	.8956	.2084	10.372	.9737	.06692	.5512	.01187	.004674
.7791	.9118	.1802	8.9714	.9788	.05784	.5253	.01331	.005239
.8621	.9259	.1553	7.7339	.9833	.04904	.4974	.01489	.005863
1.0280	.9482	.1140	5.6936	.9901	.03327	.4376	.01760	.006928
1.1525	.9607	.08966	4.4917	.9936	.02360	.3907	.01974	.007772
1.2769	.9705	.07011	3.5245	.9960	.01601	.3435	.02188	.008615
1.4429	.9801	.05019	2.5349	.9980	.008883	.2826	.02473	.009736
1.7333	.9903	.02773	1.4134	.9996	.002592	.1878	.02969	.01169
2.0236	.9954	.01554	.7951	1.0000	.0005746	.1144	.03465	.01364
2.1340	.9979	.008900	.4566	1.0000	.0002960	.06374	.03960	.01559
2.6459	.9990	.004752	.2442	1.0000	.0002960	.02924	.04526	.01782
2.9363	.9995	.002733	.1406	1.0000	.002960	.01336	.05019	.01976
3.4756	1.0000	.000941	.04842	1.0000	.002960	.002377	.05939	.02338

TABLE V. - Concluded. TYPICAL SOLUTIONS FOR COOLED INLET

(c) Station 20; ratio of nozzle to throat distance, 1.272; velocity gradient parameter, 0.1179; turbulent Prandtl number, 2.9495

Transformed boundary layer coordinate, η	Velocity ratio, f_η	Derivative of velocity ratio, $f_{\eta\eta}$	Shear-stress function, $\mathscr{P}_f$	Total enthalpy ratio, g	Derivative of total enthalpy ratio, g_η	Heat-transfer function, $\mathscr{P}_g$	Coordinate normal to nozzle surface, y	
							cm	in.
0	0	163.34	0.4801	0.5876	27.209	0.05632	0	0
.0002593	.04236	162.84	.4800	.5953	31.041	.06012	.0004851	.0001910
.0005187	.08430	160.12	.4799	.6037	34.358	.06388	.0009743	.0003836
.0007780	.1253	155.50	.4797	.6131	37.325	.06754	.001466	.0005773
.001297	.2027	142.00	.4795	.6334	40.018	.07442	.002452	.0009655
.002075	.3037	117.21	.4790	.6660	45.092	.08313	.003919	.001543
.003112	.4030	33.882	.4782	.6999	18.442	.09109	.005822	.002292
.004668	.4483	25.185	.4772	.7246	13.788	.09582	.008598	.003385
.007520	.5050	15.802	.4753	.7535	9.7850	.06987	.01359	.005350
.01141	.5542	10.256	.4725	.7769	7.6009	.06642	.02016	.007938
.01686	.5995	6.8492	.4685	.8041	5.4162	.06353	.02906	.01144
.02230	.6317	5.1280	.4643	.8269	3.7745	.06164	.03777	.01487
.03376	.6648	3.8713	.4584	.8590	2.2495	.05997	.04948	.01948
.05804	.7305	1.9436	.4389	.8972	1.1902	.05595	.08606	.03388
.08231	.7695	1.5087	.4194	.9226	.9013	.05301	.1204	.04742
.1187	.8196	1.2354	.3837	.9492	.6012	.04937	.1686	.06637
.1430	.8474	1.0559	.3576	.9620	.4630	.04683	.1982	.07804
.1670	.8709	.8918	.3310	.9719	.3505	.04416	.2260	.08896
.2158	.9074	.6255	.2797	.9848	.1946	.03872	.2764	.1088
.2522	.9273	.4784	.2444	.9904	.1235	.03461	.3106	.1223
.3008	.9469	.3378	.2029	.9949	.06716	.02928	.3523	.1387
.3493	.9608	.2423	.1676	.9974	.03661	.02438	.3907	.1538
.4221	.9748	.1518	.1247	.9991	.01498	.01811	.4435	.1746
.5192	.9859	.08511	.08256	1.0000	.004617	.01184	.5080	.2000
.6163	.9922	.04901	.05326	1.0000	.004473	.007572	.5685	.2238
.7134	.9959	.02850	.03319	1.0000	.004473	.004771	.6267	.2467
.8105	.9980	.01628	.01985	1.0000	.004473	.002965	.6833	.2690
.8833	.9990	.01051	.01310	1.0000	.004473	.002056	.7254	.2856
1.0290	1.0000	.004114	.005260	1.0000	.004473	.0009594	.8082	.3182

TABLE VI. - SUMMARY OF TURBULENT BOUNDARY-LAYER RESULTS FOR UNCOOLED INLET WITH BOUNDARY-LAYER BLEED AT NOZZLE ENTRANCE AT STAGNATION PRESSURE OF 207 NEWTONS PER SQUARE CENTIMETER (300 PSIA)

Station	Ratio of nozzle to throat distance, $x \cdot x_T$	Velocity gradient parameter, β	Shear function at wall, $\left(\frac{\mathscr{P}}{f}\right)_w$	Turbulent Prandtl number, Pr_T	Skin friction coefficient, C_f	Heat-transfer coefficient, C_q		Momentum thickness, θ		Displacement thickness, δ^*		Energy thickness, ϕ	
						g $(cm^2)(sec)$	lb/$(in.^2)(sec)$	cm	in.	cm	in.	cm	in.
2	0.0480	0.06224	1.0510	0.9726	0.006731	0.07727	0.001099	0.004064	0.001600	0.004851	0.001910	0.005169	0.002035
3	.2622	1.048	1.8627	.9844	.006218	.06742	.000959	.008141	.003205	.005537	.002180	.01727	.006800
4	.4770	2.723	2.7043	1.0222	.005837	.09203	.001309	.007442	.002930	.003874	.001525	.02350	.00925
5	.5527	3.5782	3.7158	1.0426	.005721	.09955	.001416	.006655	.002620	.003467	.001365	.02266	.00892
6	.6268	4.4261	3.8327	1.0271	.005480	.1179	.001677	.006261	.002465	.002642	.001040	.02446	.00963
7	.7021	5.883	4.4721	1.0630	.005375	.1367	.001945	.005474	.002155	.002492	.000981	.02337	.009200
8	.7774	10.22	7.2231	1.5030	.005451	.1740	.002475	.003175	.001250	.002098	.000826	.01135	.00447
9	.8825	12.79	8.8308	1.9877	.004762	.2850	.004053	.002057	.000810	.001915	.000754	.006045	.00238
10	.9675	10.10	8.1397	1.9956	.004056	.3321	.004723	.002108	.000830	.002446	.000963	.005486	.00216
11	1.000	8.826	8.6913	2.1492	.003869	.3461	.004923	.002078	.000818	.002761	.001087	.004877	.00192
12	1.0241	7.246	7.3689	2.3415	.003699	.3233	.004598	.002083	.000820	.003327	.00138	.004013	.00158
13	1.0476	5.996	6.2358	2.4739	.003547	.2924	.004159	.002159	.000850	.004008	.001578	.003520	.001386
14	1.0737	4.455	5.7585	2.4855	.003592	.2592	.003685	.002685	.001057	.005334	.00210	.003609	.001421
15	1.1201	2.317	4.3295	2.3929	.002994	.2457	.003495	.003404	.001340	.007785	.003065	.003912	.001540
16	1.2328	1.639	3.1528	2.2681	.002782	.1903	.002707	.004153	.001635	.01118	.00440	.004674	.001840
17	1.5236	0.913	1.5921	2.1081	.002560	.09836	.001399	.006020	.002370	.02306	.00908	.006477	.002550
18	2.0485	.4607	.6765	1.9689	.002438	.03761	.000535	.008966	.003530	.04981	.01961	.01033	.003950
19	2.5734	.262	.3490	1.9039	.002092	.01987	.0002826	.01255	.004940	.09246	.0364	.01303	.005130
19a	------	------	------	------	-------	------	--------	-------	-------	------	------	------	-------
20	3.1167	.0532	.2483	1.8532	.001855	.01378	.000196	.01996	.00786	.1788	.0705	.01577	.00621

TABLE VII. - SUMMARY OF TURBULENT BOUNDARY-LAYER RESULTS FOR UNCOOLED INLET AT STAGNATION PRESSURE OF 207 NEWTONS PER SQUARE CENTIMETER (300 PSIA)

Station	Ratio of nozzle to throat distance $x\ x_T$	Velocity gradient parameter, β	Shear function at wall, $(\mathcal{P}_f)_w$	Turbulent Prandtl number, Pr_T	Skin friction coefficient, C_f	Heat-transfer coefficient, C_q		Momentum thickness, θ		Displacement thickness, δ^*		Energy thickness, ϕ	
						g $(cm^2)(sec)$	lb/$(in.^2)(sec)$	cm	in.	cm	in.	cm	in.
2	0.7602	3.555	8.890	1.0000	0.005492	0.0346	0.000493	0.0335	0.0132	0.01562	0.006150	0.09804	0.03860
3	.8139	12.91	2.525	.7862	.008524	.04872	.000693	.02316	.009120	-.03797	-.01495	.2327	.09160
4	.8682	19.67	3.890	1.1508	.007621	.05885	.000837	.01318	.005190	-.03048	-.00120	.08331	.03280
5	.8873	22.79	4.596	1.2467	.007505	.06749	.000960	.01016	.00400	-.001486	-.000585	.06426	.0253
6	.9060	25.38	5.126	1.1467	.007382	.08085	.00115	.008814	.00347	-.004191	-.00165	.07747	.0305
7	.9247	30.74	5.229	1.2967	.007038	.09358	.001331	.007214	.00284	-.0008230	-.000324	.05436	.0214
8	.9439	49.20	28.486	2.6578	.007938	.1387	.001973	.003861	.00152	.002449	.000964	.01407	.00554
9	.9701	55.75	28.773	3.7236	.006017	.2325	.003307	.002540	.00100	.002644	.001041	.006058	.002385
10	.9916	41.07	25.292	3 8107	.005251	.2819	.004009	.002662	.001048	.003411	.001343	.005588	.00220
11	1.0000	35.01	22.098	3.9191	.004939	.2818	.004008	.002616	.001030	.003861	.001520	.004712	.001855
12	1.006	28.24	18.371	4.2975	.004672	.2672	.003800	.002614	.001029	.004547	.00179	.003820	.001504
13	1.012	22.98	15.265	4.5410	.004435	.2433	.003461	.002659	.001047	.005238	.00208	.003340	.001315
14	1.018	16.77	13.089	4.5260	.004208	.2266	.003223	.003112	.001225	.006756	.00266	.003340	.001315
15	1.030	8.45	10.168	4.2714	.003681	.2068	.002941	.004343	.00171	.01052	.00414	.003739	.001472
16	1.058	5.58	7.085	3.8882	.003387	.1633	.002322	.005283	.002080	.01506	.00593	.004610	.001815
17	1.132	2.690	3.299	3.3392	.003090	.08697	.001237	.007518	.00296	.03076	.01211	.006629	.00261
18	1.264	1.131	1.263	2.8367	.002906	.03508	.000499	.01229	.00484	.07468	.0294	.01080	.00425
19	1.390	.563	.6864	2.5790	.002803	.02011	.000286	.01806	.00711	.1394	.0549	.01562	.00615
19a	1.470	.310	.4964	2.4756	.002553	.01448	.000206	.02197	.00865	.1918	.0755	.01669	.00657
20	1.533	.104	.3708	2.3985	.001983	.01336	.000190	.02525	.00993	.2248	.0885	.01734	.00683

TABLE VIII. - SUMMARY OF TURBULENT BOUNDARY LAYER RESULTS FOR COOLED INLET AT STAGNATION PRESSURE OF 207 NEWTONS PER SQUARE CENTIMETER (300 PSIA)

Station	Ratio of nozzle to throat distance, x / x_T	Velocity gradient parameter, β	Shear function at wall, $(\mathcal{P}_f)_w$	Turbulent Prandtl number, Pr_T	Skin friction coefficient, C_f	Heat-transfer coefficient, C_q		Momentum thickness, θ		Displacement thickness, δ^*		Energy thickness, ϕ	
						g (cm^2)(sec)	lb $(in.^2)$(sec)	cm	in.	cm	in.	cm	in.
2	0.8776	9.428	7.5504	1.0000	0.006598	0.0326	0.000466	0.05840	0.0230	-0.00965	-0.00380	0.2400	0.0945
3	.9052	28.168	.8989	1.0000	.008268	.01758	.0002500	.02159	.00850	-.1270	-.05000	.5385	.2120
4	.9328	41.473	10.775	1.2970	.007586	.04969	.0007068	.01407	.00554	-.004597	-.001810	.09042	.03560
5	.1426	47.514	11.751	1.4689	.007522	.05788	.0008233	.01118	.00440	-.002261	-.000890	.06909	.02720
6	.1521	52.409	10.211	1.2966	.007156	.06933	.0009861	.01024	.00403	-.004801	-.00189	.07772	.03060
7	.9616	62.733	11.803	1.5439	.007115	.08092	.001151	.007595	.002990	-.001783	-.000702	.05359	.02110
8	.9714	99.383	35.687	3.6399	.006904	.1160	.001650	.003988	.001570	002870	.00113	.01171	.00461
9	.9847	111.24	40.232	5.1688	.005963	.2041	.002903	.002614	.001029	.002583	.001017	.005563	.00219
10	.9957	81.549	35.602	5.2411	.005250	.2379	.003384	.002672	.001052	.003426	.001349	.005055	.00199
11	1.0000	68.741	31.320	5.3998	.004997	.2378	.003382	.002649	.001043	.003962	.001560	.004166	.00164
12	1.003	55.212	25.545	5.9289	.004645	.2248	.003197	.002614	.001029	.004509	.001775	.003416	.001345
13	1.006	44.761	21.737	6.2656	.004522	.2056	.002925	.002736	.001077	.005385	.002120	.003020	.001189
14	1.009	32.591	20.162	6.2375	.004651	.1899	.002701	.003462	.001363	.007328	.002885	.003051	.001201
15	1.015	16.339	14.426	5.8600	.003755	.1739	.002473	.004470	.001760	.01082	.004260	.003353	.001320
16	1.030	10.660	9.8378	5.2874	.003403	.1368	.001946	.005359	.002110	.01537	.00605	.004089	.00161
17	1.067	4.977	5.154	4.4478	.003549	.07403	.001053	.009068	.003570	.03612	.01422	.006261	.002465
18	1.135	1.987	1.8042	3.6619	.003131	.02947	.0004192	.01379	.005430	.08382	.03300	.01001	.003940
19	1.202	.9502	.8602	3.2467	.002703	.01816	.0002583	.01788	.007040	.1407	.05540	.01214	.004780
19a	1.234	5127	.6051	3.0787	.002419	.01382	.0001966	.02141	.008430	.1895	.07460	.01632	.006425
20	1.272	.1179	.4801	2.9495	.002012	.01251	.0001780	.02680	.01055	.2609	.1027	.01699	.00669

TABLE IX. - SUMMARY OF TURBULENT BOUNDARY LAYER RESULTS FOR COOLED INLET AT STAGNATION PRESSURE OF 20.7 NEWTONS PER SQUARE CENTIMETER (30.0 PSIA)

Station	Ratio of nozzle to throat distance, x/x_T	Velocity gradient parameter, β	Shear function at wall $(\mathcal{P}_f)_w$	Turbulent Prandtl number, Pr_T	Skin friction coefficient C_f	Heat-transfer coefficient C_q		Momentum thickness, θ		Displacement thickness, δ^*		Energy thickness, ϕ	
						g $(cm^2)(sec)$	lb $(in.^2)(sec)$	cm	in.	cm	in.	cm	in.
2	0.8776	9.4284	3.6977	1.0000	0.01116	0.005685	0.00008086	0.1143	0.04500	-0.08103	-0.03190	0.4923	0.1938
3	.9052	28.169	.2544	1.0000	.01405	.003754	.00005340	.04636	.01825	-.4800	-.1890	1.3210	.5200
4	.9328	41.473	4.6050	1.2970	.01439	.009203	.0001309	.03233	.01273	-.05130	-.02020	.2186	.08605
5	.9426	47.514	5.9079	1.4689	.01426	.01252	.0001781	.02532	.00997	-.04623	-.01820	.1892	.0745
6	.9521	52.409	4.5930	1.2966	.01369	.01162	.0001653	.02266	.00892	-.04496	-.0177	.1770	.0697
7	.9616	62.733	4.7898	1.5424	.01254	.01797	.0002556	.02215	.00872	-.03531	-.01390	.1534	.0604
8	.9714	99.383	22.141	3.6399	.01372	.02302	.0003274	.008115	.003195	.0008179	.000322	.02570	.01012
9	.9847	111.24	24.95	5.1688	.01169	.04132	.0005877	.006096	.002400	.003211	.001264	.01181	.004650
10	.9957	81.549	21.316	5.2511	009972	.04569	.0006499	.006210	.002445	.004928	.001940	.01064	.004190
11	1.0000	68.741	18.934	5.3998	.009554	.04577	.0006510	.006058	.002385	.006058	.002385	.009093	.003580
12	1.003	55.212	16.093	5.9289	.009253	.04377	.0006226	.005956	.002345	.007518	.002960	.007620	.003000
13	1.006	44.761	13.576	6.2656	.008981	.04163	.0005921	006185	.002435	.009398	.003700	.006998	.002755
14	1.009	32.591	11.164	6.2375	.008143	.03822	.0005436	.006617	.002605	.01175	.004625	.006858	.002700
15	1.015	16.339	8.8498	5.8600	.007284	.03286	.0004674	.009296	.003660	.01943	.00765	.007468	.002940
16	1.030	10.660	6.0207	5.2874	.006587	.02541	.0003614	.01077	.004240	.02779	.01094	.008788	.003460
17	1.067	4.977	2.7890	4.4478	006073	.01401	.0001992	.01605	.006320	.05969	.02350	.01308	.00515
18	1.135	1.987	1.0435	3.6618	.005726	.005945	.00008456	.02538	.009991	.1473	.05800	.02102	.008275
19	1.202	.9502	.5293	3.2467	.005259	.003387	.00004817	.03485	.01372	.2743	.1080	.02819	.01110
20	1.272	.1179	.3190	2.9495	.004216	.002430	.00003456	.04572	.01800	.4166	.1640	.03330	.01311

TABLE X. - SUMMARY OF LAMINAR BOUNDARY LAYER RESULTS FOR COOLED INLET AT STAGNATION PRESSURE OF 20.65 NEWTONS PER SQUARE CENTIMETER (30 PSIA)

[Laminar Prandtl number, 0.71]

Station	Ratio of nozzle to throat distance, x/x_T	Velocity gradient parameter, β	Shear function at wall, $(\mathscr{P}_f)_w$	Skin friction coefficient, C_f	Heat-transfer coefficient, C_q		Momentum thickness, θ		Displacement thickness, δ^*		Energy thickness, ϕ	
					$g/(cm^2)(sec)$	$lb/(in.^2)(sec)$	cm	in.	cm	in.	cm	in.
2	0.8776	9.4284	1.3849	0.004958	0.00144	0.00002054	0.03505	0.01380	-0.004816	-0.001896	0.1283	0.0505
3	.9052	28.169	.2885	.008524	.000806	.00001146	.009800	.00386	-.13310	-.05240	.3099	.1220
4	.9328	41.473	1.5921	.007538	.003029	.00004308	.007061	.002780	-.01803	-.007100	.07264	.02860
5	.9426	47.514	1.8625	.007129	.003785	.00005384	.006083	.002395	-.01346	-.005300	.05715	.02250
6	.9521	52.409	1.0070	.006026	.003772	.00005365	.007061	.002780	-.01308	-.005150	.05740	.02260
7	.9616	62.733	1.0958	.005672	.004944	.00007032	.006426	.002530	-.008204	-.003230	.04255	.01675
8	.9714	99.383	5.0912	.005867	.01282	.0001823	.004178	.001645	.0003683	.000145	.01389	.005470
9	.9847	111.24	8.0314	.004479	.02361	.0003358	.002413	.000950	.001214	.000478	.006566	.002585
10	.9957	81.549	5.2361	.003352	.02415	.0003435	.002106	.0008290	.001651	.0006500	.005347	.002105
11	1.0000	68.741	5.33448	.003159	.02468	.0003511	.002007	.0007900	.002019	.000795	.004712	.001855
12	1.003	55.212	4.3930	.003006	.02468	.0003511	.001943	.0007650	.002598	.001023	.004102	.001615
13	1.006	44.761	3.6217	.002883	.02345	.0003335	.001956	.0007700	.003221	.001268	.003769	.001484
14	1.009	32.591	2.8966	.002608	.02128	.0003027	.002083	.0008200	.004026	.001585	.003708	.001460
15	1.015	16.339	2.4941	.002053	.01757	.0002499	.002492	.0009810	.005867	.002310	.003858	.001519
16	1.030	10.660	1.7266	.001889	.01292	.0001838	.003018	.001188	.008509	.003350	.004437	.001747
17	1.067	4.977	0.8282	.001803	.006501	.00009246	.004415	.001738	.01923	.00757	.005931	.002335
18	1.135	1.987	.3258	.001788	.002601	.00003699	.007315	.00288	.05207	.02050	.009119	.003590
19	1.202	.9502	.1723	.001713	.001390	.00001977	.01048	.004125	.1039	.04090	.01219	.004800
20	1.272	.1179	.08717	.001155	.000934	.00001329	.01524	.006000	.1869	.07360	.01516	.00597

"The aeronautical and space activities of the United States shall be conducted so as to contribute . . . to the expansion of human knowledge of phenomena in the atmosphere and space. The Administration shall provide for the widest practicable and appropriate dissemination of information concerning its activities and the results thereof."

— NATIONAL AERONAUTICS AND SPACE ACT OF 1958

NASA SCIENTIFIC AND TECHNICAL PUBLICATIONS

TECHNICAL REPORTS: Scientific and technical information considered important, complete, and a lasting contribution to existing knowledge.

TECHNICAL NOTES: Information less broad in scope but nevertheless of importance as a contribution to existing knowledge.

TECHNICAL MEMORANDUMS: Information receiving limited distribution because of preliminary data, security classification, or other reasons.

CONTRACTOR REPORTS: Scientific and technical information generated under a NASA contract or grant and considered an important contribution to existing knowledge.

TECHNICAL TRANSLATIONS: Information published in a foreign language considered to merit NASA distribution in English.

SPECIAL PUBLICATIONS: Information derived from or of value to NASA activities. Publications include conference proceedings, monographs, data compilations, handbooks, sourcebooks, and special bibliographies.

TECHNOLOGY UTILIZATION PUBLICATIONS: Information on technology used by NASA that may be of particular interest in commercial and other non-aerospace applications. Publications include Tech Briefs, Technology Utilization Reports and Technology Surveys.

Details on the availability of these publications may be obtained from:

SCIENTIFIC AND TECHNICAL INFORMATION OFFICE

NATIONAL AERONAUTICS AND SPACE ADMINISTRATION

Washington, D.C. 20546